CANCER

Tumor-derived semaphorin 4A improves PD-1–blocking antibody efficacy by enhancing CD8$^+$ T cell cytotoxicity and proliferation

**Yujiro Naito[1,2,3], Shohei Koyama[1,2,4]*, Kentaro Masuhiro[1,3]†, Takashi Hirai[3,5]†, Takeshi Uenami[6], Takako Inoue[7], Akio Osa[1], Hirotomo Machiyama[1], Go Watanabe[4], Nicolas Sax[8], Jordan Villa[8], Yumi Kinugasa-Katayama[9], Satoshi Nojima[10], Moto Yaga[1,3], Yuki Hosono[1,11,12], Daisuke Okuzaki[13,14,15], Shingo Satoh[1,3], Takeshi Tsuda[5], Yoshimitsu Nakanishi[1,3], Yasuhiko Suga[1], Takayoshi Morita[1,3], Kiyoharu Fukushima[1,16], Masayuki Nishide[1,3], Takayuki Shiroyama[1], Kotaro Miyake[1], Kota Iwahori[1], Haruhiko Hirata[1], Izumi Nagatomo[1], Yukihiro Yano[6], Motohiro Tamiya[7], Toru Kumagai[7], Norihiko Takemoto[5], Hidenori Inohara[5], Sho Yamasaki[11,12], Kazuo Yamashita[8], Taiki Aoshi[9], Esra A. Akbay[17], Naoki Hosen[14,18,19], Yasushi Shintani[20], Hyota Takamatsu[1,3], Masahide Mori[6], Yoshito Takeda[1], Atsushi Kumanogoh[1,2,3,14,15,21,22]*

Immune checkpoint inhibitors (ICIs) have caused revolutionary changes in cancer treatment, but low response rates remain a challenge. Semaphorin 4A (Sema4A) modulates the immune system through multiple mechanisms in mice, although the role of human Sema4A in the tumor microenvironment remains unclear. This study demonstrates that histologically Sema4A-positive non–small cell lung cancer (NSCLC) responded significantly better to anti–programmed cell death 1 (PD-1) antibody than Sema4A-negative NSCLC. Intriguingly, SEMA4A expression in human NSCLC was mainly derived from tumor cells and was associated with T cell activation. Sema4A promoted cytotoxicity and proliferation of tumor-specific CD8$^+$ T cells without terminal exhaustion by enhancing mammalian target of rapamycin complex 1 and polyamine synthesis, which led to improved efficacy of PD-1 inhibitors in murine models. Improved T cell activation by recombinant Sema4A was also confirmed using isolated tumor-infiltrating T cells from patients with cancer. Thus, Sema4A might be a promising therapeutic target and biomarker for predicting and promoting ICI efficacy.

INTRODUCTION

Immune checkpoint inhibitors (ICIs) have emerged as a promising treatment for multiple types of advanced cancer. However, only a fraction of patients exhibit a clinical response to ICIs, underscoring that predictive biomarkers of ICI response and additional targeted therapies are necessary to improve their efficacy (*1*). ICIs play a key role in improving T cell priming by antigen-presenting cells and in reinvigorating tumor-infiltrating T cells in lymphoid organs and the tumor microenvironment (TME) (*2*). While clinically approved ICIs block coinhibitory signaling in T cells, costimulatory molecules involved in T cell activation, including OX40 and 4-1BB, can serve as potential therapeutic targets in conjunction with ICIs (*3*), even in noninflamed tumors as we previously reported (*4*). Moreover, the administration of anti-OX40 and anti–4-1BB antibodies enhanced programmed cell death 1 (PD-1)–blocking treatment by rescuing exhausted CD8$^+$ T cells in chronic infection models (*5*, *6*).

The effector function and proliferation of PD-1$^+$CD8$^+$ T cells without terminal exhaustion phenotypes are essential for the antitumor immune response provoked by PD-1 inhibitors (*7*). The balance between the transcriptional checkpoints thymocyte

[1]Department of Respiratory Medicine and Clinical Immunology, Graduate School of Medicine, Osaka University, Suita, Osaka, Japan. [2]Department of Immunology and Molecular Medicine, Graduate School of Medicine, Osaka University, Suita, Osaka, Japan. [3]Department of Immunopathology, World Premier International Research Center (WPI), Immunology Frontier Research Center (IFReC), Osaka University, Suita, Osaka, Japan. [4]Division of Cancer Immunology, Research Institute/Exploratory Oncology Research and Clinical Trial Center (EPOC), National Cancer Center, Kashiwa,Chiba, and Tokyo, Japan. [5]Department of Otorhinolaryngology–Head and Neck Surgery, Graduate School of Medicine, Osaka University, Suita, Osaka, Japan. [6]Department of Thoracic Oncology, National Hospital Organization, Osaka Toneyama Medical Center, Toyonaka, Osaka, Japan. [7]Department of Thoracic Oncology, Osaka International Cancer Institute, Osaka, Japan. [8]KOTAI Biotechnologies Inc., Suita, Osaka, Japan. [9]Department of Cellular Immunology, Research Institute for Microbial Diseases (RIMD), Osaka University, Suita, Osaka, Japan. [10]Department of Pathology, Graduate School of Medicine, Osaka University, Suita, Osaka, Japan. [11]Laboratory of Molecular Immunology, WPI, IFReC, Osaka University, Suita, Osaka, Japan. [12]Department of Molecular Immunology, RIMD, Osaka University, Suita, Osaka, Japan. [13]Single Cell Genomics, Human Immunology, WPI, IFReC, Osaka University, Suita, Osaka, Japan. [14]Integrated Frontier Research for Medical Science Division, Institute for Open and Transdisciplinary Research Initiatives (OTRI), Osaka University, Suita, Osaka, Japan. [15]Center for Infectious Diseases for Education and Research (CiDER), Osaka University, Suita, Osaka, Japan. [16]Laboratory of Host Defense, WPI, IFReC, Osaka University, Suita, Osaka, Japan. [17]Department of Pathology, University of Texas Southwestern Medical Center, Dallas, TX, USA. [18]Department of Hematology and Oncology, Graduate School of Medicine, Osaka University, Suita, Osaka, Japan. [19]Laboratory of Cellular Immunotherapy, WPI, IFReC, Osaka University, Suita, Osaka, Japan. [20]Department of General Thoracic Surgery, Graduate School of Medicine, Osaka University, Suita, Osaka, Japan. [21]Japan Agency for Medical Research and Development–Core Research for Evolutional Science and Technology (AMED-CREST), Osaka University, Suita, Osaka, Japan. [22]Center for Advanced Modalities and DDS (CAMaD), Osaka University, Suita, Osaka, Japan.
*Corresponding author. Email: kumanogo@imed3.med.osaka-u.ac.jp (A.K.); koyama@imed3.med.osaka-u.ac.jp (S.K.)
†These authors contributed equally to this work.

selection-associated high mobility group box (TOX) and T cell factor 1 (TCF1) plays a key role in defining the developmental hierarchy for exhausted $CD8^+$ T cells (*8*, *9*), which is strongly linked to the revitalization of effector T cells after ICI treatment (*10*, *11*). The mammalian target of rapamycin (mTOR) kinase pathway regulates reprogramming of anabolic metabolism in T cells, and mTOR complex 1 (mTORC1) is required for cell cycle entry and for adapting to early metabolic changes upon T cell receptor (TCR) activation (*12*). The asymmetric partitioning of mTORC1 activity after naïve $CD8^+$ T cell activation contributes to the generation of effector and memory $CD8^+$ T cells (*13*), and up-regulation of mTORC1-dependent hypoxia-inducible factor 1 is required to sustain glucose metabolism and glycolysis in effector $CD8^+$ T cells (*14*). Together, these findings suggest that mTORC1 activity is essential for the effector function and proliferation of antigen-specific $CD8^+$ T cells.

Semaphorins are a large family of secreted and membrane-bound glycoproteins that were initially implicated in axon guidance and neural development (*15*). Accumulating evidence indicates that semaphorins play multiple roles in immune responses such as immune cell activation, differentiation, and migration (*16*–*18*). We reported that semaphorin 4A (Sema4A) on dendritic cells (DCs) induced T cell priming and T helper 1 (T_H1) differentiation in $CD4^+$ T cells (*19*, *20*) and recently demonstrated that Sema4A was able to induce $CD8^+$ T cell activation, which played an important role in the interleukin-33–induced antitumor response (*21*). Sema4A can be expressed by various cell types, including myeloid cells, T cells (*22*, *23*), and cancer cells (*24*–*26*) (https://depmap.org/portal/gene/SEMA4A?tab=characterization). Immune cell–derived Sema4A has also been reported to be required for the function and stability of regulatory T cells (T_{regs}) (*27*, *28*). These previous findings, however, are based on the results of murine experiments and cell line experiments, and the role of Sema4A in humans, especially in the TME, remains unclear.

In this study, we performed an initial analysis of a previously published dataset and The Cancer Genome Atlas (TCGA) dataset. We found that *SEMA4A* was mainly expressed by epithelial cells and tumor cells, and increased *SEMA4A* expression was associated with a favorable prognosis and with T cell activation. We then conducted a retrospective multicenter cohort study and showed that Sema4A-positive non–small cell lung cancers (NSCLCs) exhibited a significantly better response to first-line anti–PD-1 monotherapy than Sema4A-negative NSCLCs. Preclinical murine models demonstrated that Sema4A expressed by tumor cells ameliorated antitumor function and proliferation of $CD8^+$ T cells by promoting mTORC1–S6 kinase (S6K) signaling and polyamine synthesis without inducing the exhaustion phenotype. Recombinant Sema4A (rSema4A) increased the effector function of tumor-infiltrating $CD8^+$ T cells isolated from both murine and human tumors in vitro. In addition, administration of rSema4A improved the therapeutic efficacy of anti–PD-1 antibodies in vivo. Thus, Sema4A expression in the TME can be a vital biomarker as well as a potential therapeutic target for improvement of prediction and response to ICIs.

RESULTS

SEMA4A expression is associated with genes related to T cell infiltration and activation and with increased ICI efficacy in patients with cancer

We initially investigated TCGA datasets of lung adenocarcinoma (LUAD) and head and neck squamous cell carcinoma (HNSCC) regarding the relation between *SEMA4A* mRNA expression and 5-year overall survival (OS). Each dataset was divided into two groups according to *SEMA4A* expression: *SEMA4A*-high (upper 50%) and *SEMA4A*-low (lower 50%). The 5-year OS rate was significantly higher in the *SEMA4A*-high group than in the *SEMA4A*-low group for both LUAD and HNSCC (Fig. 1A). Moreover, the same datasets were equally divided into three groups according to *SEMA4A* expression, and 5-year OS was compared between the groups with the highest (upper 33%) versus lowest (lower 33%) expression. The difference between these two groups was more pronounced than that between the upper 50% and lower 50% groups (fig. S1A). To identify the gene signatures and pathways associated with *SEMA4A* expression, we used gene set enrichment analysis (GSEA) to compare *SEMA4A*-high and *SEMA4A*-low tumors. Various gene signatures, including those related to T cell activation and differentiation, were significantly enriched in *SEMA4A*-high tumors compared to *SEMA4A*-low tumors (Fig. 1B). We also analyzed TCGA data of skin cutaneous melanoma (SKCM) and found that SKCM had a similar phenotype as LUAD and HNSCC (fig. S1, B and C). Moreover, evaluation of published data (*29*) demonstrated that the *SEMA4A*-high group had better survival than the *SEMA4A*-low group in patients with melanoma treated with anti–PD-1 antibody, though the *P* value was not significant ($P = 0.061$) (fig. S1D).

We next used single-cell RNA sequencing (scRNAseq) data of NSCLC samples obtained from the National Center for Biotechnology Information (NCBI) Gene Expression Omnibus (GEO) (GSE131907) to determine which cell population predominantly expressed *SEMA4A* in the TME (*24*). DCs, tumor-associated macrophages (TAMs), and epithelial cells in the TME have a higher percentage of *SEMA4A*-expressing populations than other subsets (fig. S2A), and the expression levels of *SEMA4A* are comparable among DCs, TAMs, and epithelial cells (fig. S2B). The number of *SEMA4A*-expressing cells in epithelial cells was much higher than that in DCs and TAMs (fig. S2B), indicating that *SEMA4A* is mainly expressed by epithelial cells, including tumor cells, in the TME.

To clarify which Sema4A-expressing cells in the TME are involved in modulating the sensitivity to ICI treatment, we investigated two murine models that differed regarding the time course of tumor development. The first model was a genetically engineered mouse model (GEMM) of LUAD consisting of $Kras^{G12D}$-mutated mice with or without *Sema4a*-deficient lung cancers (*Kras* and *Kras*/*Sema4a* KO). In this model, it takes several months for visible tumors to develop. The second model was a syngeneic LUAD model involving subcutaneous transplantation of a $Kras^{G12D}$-mutated, *Tp53*-deficient LUAD cell line (KP) (*30*) with ovalbumin (OVA) expression (KP^{OVA}). Because cancer cells did not express Sema4A in either of these models, the impact of Sema4A expression by immune cells and stromal cells on the tumor growth and tumor immune microenvironment was evaluated. *Kras*/*Sema4a* KO mice showed significantly worse prognosis than *Kras* mice (fig. S3A). Pathological evaluation revealed a

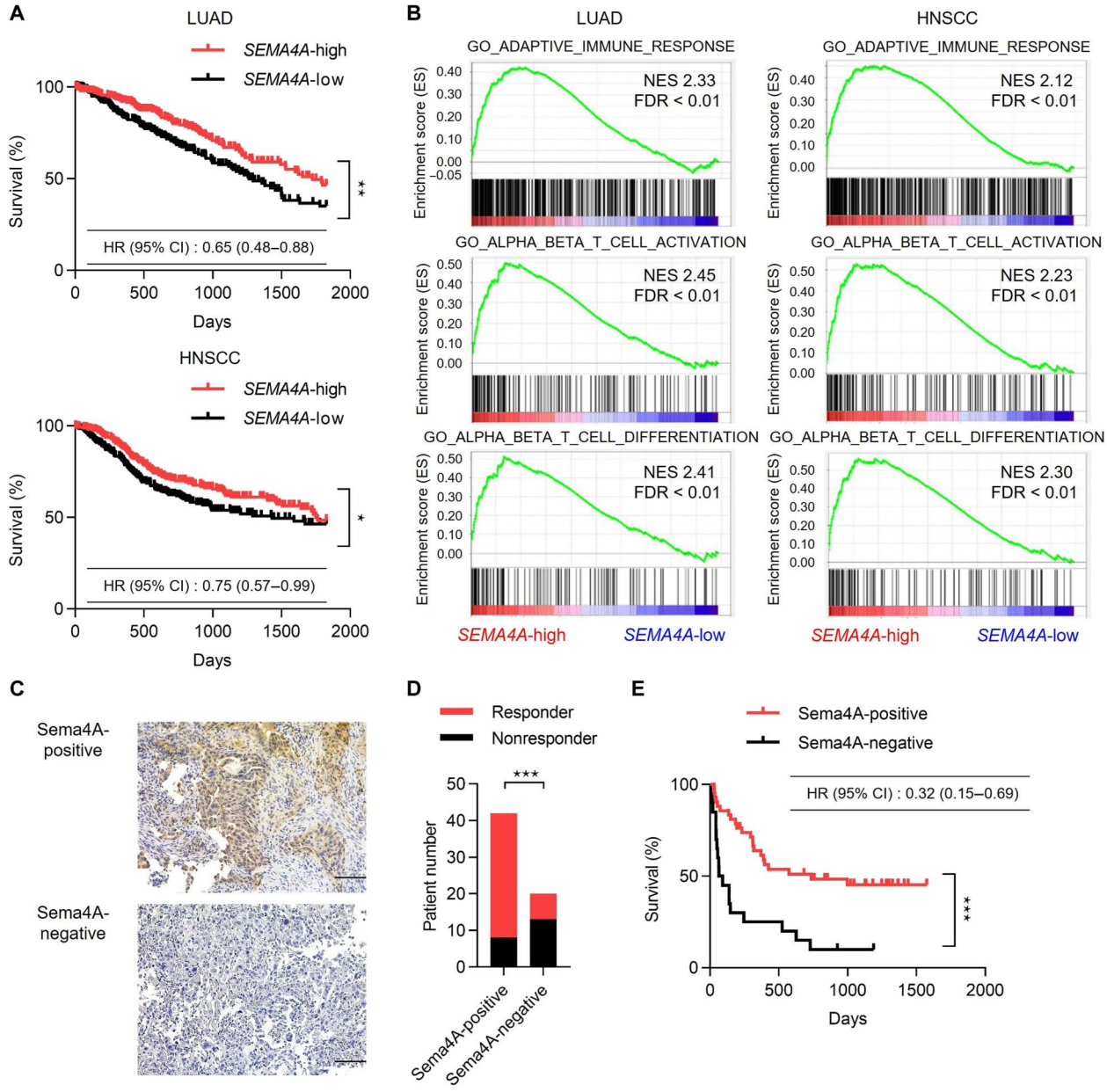

Fig. 1. Sema4A expression in tumors is linked to preferable prognosis and T cellactivation gene signatures in patients with NSCLC and HNSCC. (**A**) OS curves of patients in the TCGA dataset who were followed up for 5 years were compared between the *SEMA4A*-high (red, upper 50%) and *SEMA4A*-low (black, lower 50%) groups for LUAD ($n = 253$ versus 252, $^{**}P < 0.01$, log-rank test) and HNSCC ($n = 259$ versus 260, $^{*}P < 0.05$, log-rank test). HR, hazard ratio; CI, confidence interval. (**B**) GSEA results of the TCGA dataset showing representative gene signatures that are significantly enriched in *SEMA4A*-high tumors compared to *SEMA4A*-low tumors. NES, normalized enrichment score; FDR, false discovery rate. (**C**) IHC staining for Sema4A in NSCLC specimens collected before the initiation of PD-1–blocking treatment. Sema4A staining (brown). Magnification, ×20. Scale bar, 100 μm. (**D**) Number of cases who responded or did not respond to the anti–PD-1 antibody pembrolizumab in the Sema4A-positive group (34 responders of 42 total cases) versus the Sema4A-negative group (7 responders of 20 total cases) ($^{***}P < 0.001$, Fisher's exact test). Red represents responders, who completed six or more courses, and black represents nonresponders, who completed fewer than six courses. (**E**) PFS of patients with NSCLC treated with pembrolizumab was compared between Sema4A-positive (red, $n = 42$) and Sema4A-negative (black, $n = 20$) groups. $^{***}P < 0.001$, log-rank test.

larger tumor size and a smaller number of tumor-infiltrating $CD8^+$ T cells in *Kras*/*Sema4a* KO mice than in *Kras* mice (fig. S3, B to D). In the syngeneic model, KP^{OVA} cell lines were subcutaneously injected into wild-type (WT) and *Sema4a* knockout (KO) mice. There was a trend toward faster tumor growth in *Sema4a* KO mice than in WT mice, although the difference was not significant (fig. S4, A and B). On the basis of these findings in two murine models without cancer cell Sema4A expression, *Sema4a* deficiency in both immune cells and stromal cells was thought to have a modest impact on antitumor immunity. Therefore, it might take longer for a significant difference in tumor burden to be detected in the GEMM than in the syngeneic model.

Sema4A expressed by natural killer cells, DCs, and TAMs has a modest effect on the CD8$^+$ T cell immune response

We evaluated the role of Sema4A in natural killer (NK) cells and DCs, both of which are involved in antitumor immunity, and DC-derived Sema4A was reported to be important for priming CD4$^+$T$_H$ cells (*20*). We characterized NK cells from WT and *Sema4a* KO mice under normal conditions. The expression levels of the NK-activating receptors NKG2D and DNAM1 were comparable between WT and *Sema4a* KO mice (fig. S5A). A chromium-51 (^{51}Cr)–release assay using YAC-1 and KP cells as targets also exhibited no significant difference between WT and *Sema4a* KO mice (fig. S5B), suggesting that Sema4A is unnecessary for NK cell activation and cytotoxic function. For DCs generated with granulocyte-macrophage colony-stimulating factor (GM-CSF) (GM-DCs) or Flt3L (FL-DCs) from WT and *Sema4a* KO mice, maturation and activation markers were comparable between the two types of mice (fig. S6, A and B). The expression of Sema4A in DCs was induced by interferon-γ (IFN-γ) and several Toll-like receptor ligands. In GM-DCs, Pam3CSK4 induced the strongest Sema4A expression (fig. S7, A and B). When OT-1 CD8$^+$ T cells were cocultured with activated WT DCs expressing increased Sema4A or *Sema4a* KO DCs, no significant difference was detected in T cell proliferation (fig. S7, C and D). We also isolated Sema4A-expressing TAMs (CD45$^+$ F4/80$^+$) from KP^{OVA} tumors (fig. S8A) and evaluated whether TAMs loaded with OVA peptide functioned as antigen-presenting cells, like GM-DCs, to promote OT-I CD8$^+$ T cell proliferation. Consistent with a recent report (*31*), the proliferation of OVA-specific CD8$^+$ T cells was barely induced by TAMs (fig. S8B). Together, there was little evidence that Sema4A on NK cells, DCs, or TAMs promoted the CD8$^+$ T cell immune response, including in the TME.

Sema4A-expressing tumor cells enhance the proliferative and effector functions of antigen-specific CD8$^+$ T cells

We investigated the role of Sema4A in the TME in terms of patients' clinical responses to ICI. We originally performed immunohistochemistry (IHC) of Sema4A in NSCLC specimens (n = 62) before initiating first-line treatment with the anti–PD-1 antibody pembrolizumab. Patient characteristics are described in table S1. Sema4A staining by IHC was classified as positive or negative on the basis of Sema4A expression in tumor cells (Fig. 1C), because by performing multiplex IHC (mIHC) with representative formalin-fixed paraffin-embedded specimens from patients with NSCLC in this cohort, we confirmed that cells expressing Sema4A in the TME were predominantly cancer cells. However, TAMs and DCs showed high Sema4A expression, which was consistent with the scRNAseq data (fig. S9, A and B). Compared to patients with SemaA4-negative NSCLCs, those with Sema4A-positive NSCLCs showed a significantly higher frequency of responders (Fig. 1D) and significantly longer progression-free survival (PFS) (Fig. 1E).

We then investigated the role of tumor cell Sema4A in murine models. We transduced Sema4A into two cell lines, KP and oral squamous cell carcinoma 2 (MOC2). These cell lines were also transduced with OVA (KP^{OVA} and MOC2^{OVA}) with or without Sema4A (OVA-mock or OVA-Sema4A). These cell lines were injected into mice via subcutaneous and intratracheal routes. After subcutaneous injection, tumor growth was significantly faster in KP$^{OVA\text{-}mock}$ cells than in KP$^{OVA\text{-}Sema4A}$ cells (Fig. 2, A and B). To further evaluate the correlation between Sema4A expression level and tumor growth inhibition, we sorted low and high Sema4A-expressing cells (KP$^{OVA\text{-}Sema4A\text{-}low}$ and KP$^{OVA\text{-}Sema4A\text{-}high}$) from KP$^{OVA\text{-}Sema4A}$ (fig. S10A). H2Kb SIINFEKL induction by IFN-γ and tumor growth in vitro were comparable between KP$^{OVA\text{-}mock}$, KP$^{OVA\text{-}Sema4A\text{-}low}$ and KP$^{OVA\text{-}Sema4A\text{-}high}$ cells (fig. S10, B and C). We confirmed that the Sema4A expression level in the KP^{OVA} cell line was correlated with tumor growth inhibition (Fig. 2, C and D). Similar results were also obtained in MOC2^{OVA}-injected mice (fig. S10, D to H). In addition, IHC staining of tumors revealed that more CD8$^+$ and granzyme B$^+$ cells infiltrated into KP$^{OVA\text{-}Sema4A}$ tumors than into KP$^{OVA\text{-}mock}$ tumors (Fig. 2, E to H). For intratracheal injection, survival was significantly longer in mice injected with KP$^{OVA\text{-}Sema4A}$ compared to KP$^{OVA\text{-}mock}$ (Fig. 2I). To further investigate the contribution of endogenous Sema4A expression to antitumor immunity in tumor cells, we confirmed the expression of endogenous Sema4A in a leukemia cell line (WEHI-3B), which we transplanted into WT mice (*32*). We used short hairpin RNA (shRNA) to develop *Sema4a* knockdown cells (WEHI-3B^{4aKD}) and its control cell line (WEHI-3B^{mock}) (fig. S11A) and evaluated their growth in vivo. Consistent with Sema4A overexpression, *Sema4a* KD tumor showed worse clinical outcome (fig. S11, B and C).

We evaluated the immunological profile of immune cells isolated from KP$^{OVA\text{-}mock}$ and KP$^{OVA\text{-}Sema4A}$ tumors at day 8 after subcutaneous injection (Fig. 3A). OVA-specific responses, cytotoxic function, and differentiation markers, such as CD107a and Tbet, in tumor-infiltrating CD8$^+$ T cells were significantly increased in KP$^{OVA\text{-}Sema4A}$ tumors compared to KP$^{OVA\text{-}mock}$ tumors (Fig. 3, B and C). PD-1 positivity in T cells was elevated, whereas the positivity of terminal exhaustion markers such as LAG3 and TOX was not (Fig. 3D). These results were consistent with those from models using cancer cells originally expressing Sema4A (fig. S11, D to F). While the number of CD4$^+$ T cells was comparable, the number of T$_{regs}$ was significantly decreased in KP$^{OVA\text{-}Sema4A}$ tumors compared to KP$^{OVA\text{-}mock}$ tumors (Fig. 3B). Regarding other immune cell populations, NK cells, granulocytic myeloid-derived suppressor cells (G-MDSCs), and inflammatory monocytes were also decreased in KP$^{OVA\text{-}Sema4A}$ tumors compared to KP$^{OVA\text{-}mock}$ tumors (fig. S12). To evaluate whether tumor-derived Sema4A modulates the tumor immune microenvironment by interacting with specific immune cells, we injected KP$^{OVA\text{-}mock}$ and KP$^{OVA\text{-}Sema4A}$ tumors into *Rag2* KO mice or mice treated with CD8-depletion antibodies. The growth inhibition of KP$^{OVA\text{-}Sema4A}$ tumors was abrogated (Fig. 3, E and F). In addition, a metastatic lung cancer model using intravenous injection of KP cell lines (not expressed with OVA) with or without Sema4A overexpression, in which NK cells play a major role in tumor growth inhibition (*33*), did not show any difference between the growth of KP^{mock} and KP^{Sema4A} tumors (fig. S13, A and B).

To investigate whether Sema4A on tumors modulates the sensitivity to anti–PD-1–blocking treatment, we monitored the effect of this treatment on tumor growth after subcutaneous injection of KP$^{OVA\text{-}mock}$ and KP$^{OVA\text{-}Sema4A}$. After treatment, the volume of KP$^{OVA\text{-}Sema4A}$ tumors was significantly lower than that of KP$^{OVA\text{-}mock}$ tumors (Fig. 4A). We isolated tumor-infiltrating CD8$^+$ T cells from KP$^{OVA\text{-}mock}$ tumors and stimulated these cells with anti-CD3 antibody with or without rSema4A. Both the OVA-specific T cell count and IFN-γ production were significantly upregulated after treatment with anti-CD3 antibody and rSema4A

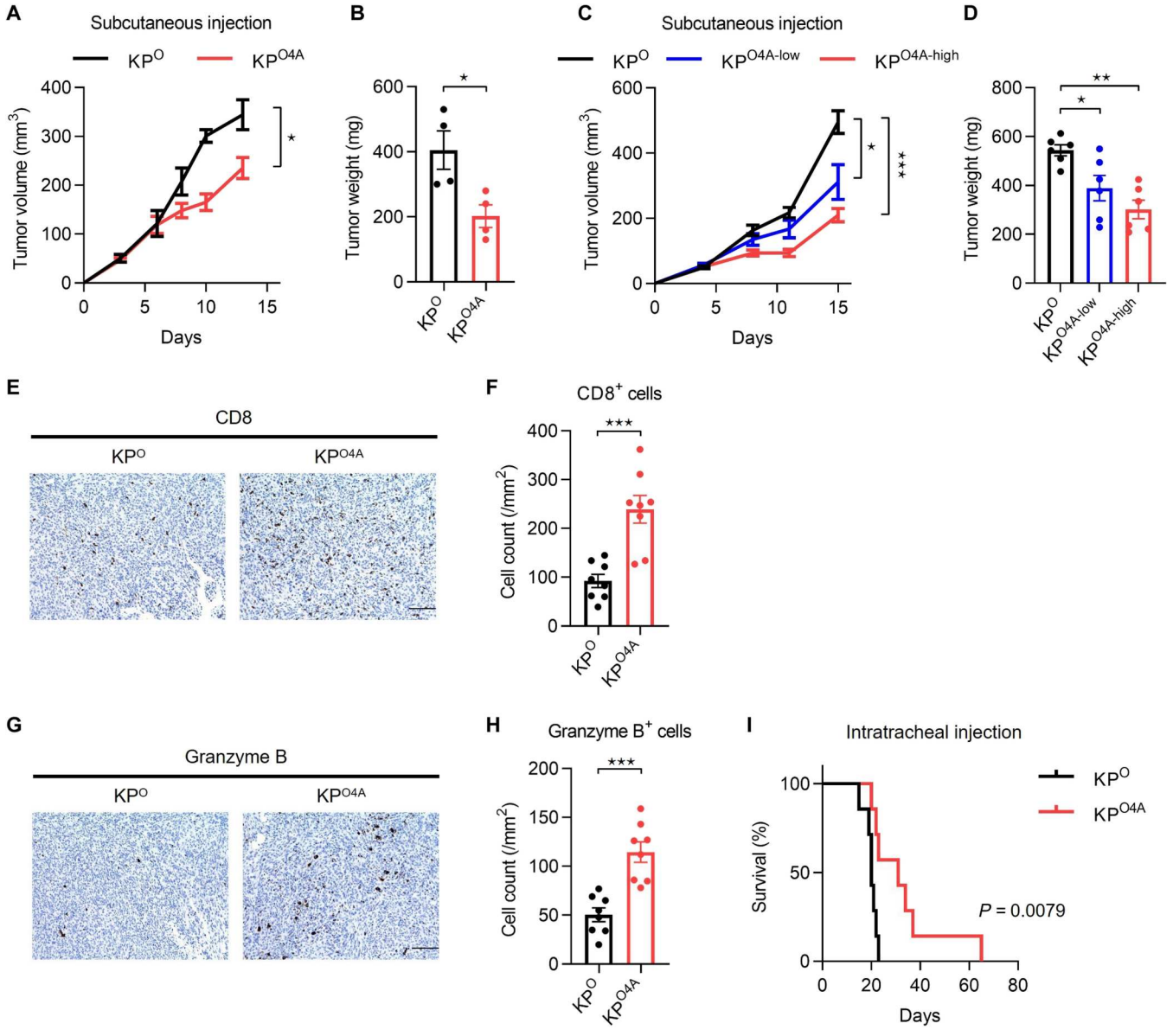

Fig. 2. Sema4A expression in cancer cells impedes tumor progression in murine models. (**A**) Tumor volume and (**B**) tumor weight in a syngeneic murine model are shown. Mice were administered KP^{OVA} with or without Sema4A overexpression [OVA-mock (O), black; OVA-Sema4A (O4A), red]. $n = 4$ per group, $^*P < 0.05$, Student's t test. The experiment was performed three times with similar results. (**C**) Tumor volume and (**D**) tumor weight in a syngeneic murine model are shown. Mice were administered KP^{O} or Sema4A overexpression with different expression levels [O, black; OVA-Sema4A-low (O4A-low), blue or OVA-Sema4A-high (O4A-high), red]. $n = 6$ per group, $^*P < 0.05$, $^{**}P < 0.01$, $^{***}P < 0.001$, one-way analysis of variance (ANOVA). The experiment was performed three times with similar results. (**E**) CD8 staining (brown) of tumors in a subcutaneous tumor model. Magnification, ×20. Scale bar, 100 μm. (**F**) $CD8^+$ cell count in tumors were compared between KP^{O} and KP^{O4A}. $n = 8$ per group, $^{***}P < 0.001$, Student's t test. (**G**) Granzyme B staining (brown) of tumors in the subcutaneous tumor model. Magnification, ×20. Scale bar, 100 μm. (**H**) Granzyme B^+ cell count in tumors were compared between KP^{O} and KP^{O4A}. $n = 8$ per group, $^{***}P < 0.001$, Student's t test. (**I**) Kaplan-Meier survival curves of mice in an intratracheal injection model administered KP^{O} or KP^{O4A}. $n = 7$ per group, $P = 0.0079$, log-rank test. The experiment was performed three times with similar results. Results are expressed as the mean ± SEM.

(Fig. 4, B and C), and this was confirmed by RNA sequencing data (Fig. 4D). We also performed a killing assay using OT-1 cells as effector cells and $KP^{OVA\text{-}mock}$ or $KP^{OVA\text{-}Sema4A}$ cells as target cells and found that $KP^{OVA\text{-}Sema4A}$ cells highly induced the killing activity of antigen-specific T cells compared to $KP^{OVA\text{-}mock}$ cells (Fig. 4E). Moreover, rSema4A partially improved the killing activity of OT-1 cells in the same assay system (Fig. 4E). These results indicate that Sema4A enhances antitumor immunity by activating antigen-specific $CD8^+$ T cells in the TME.

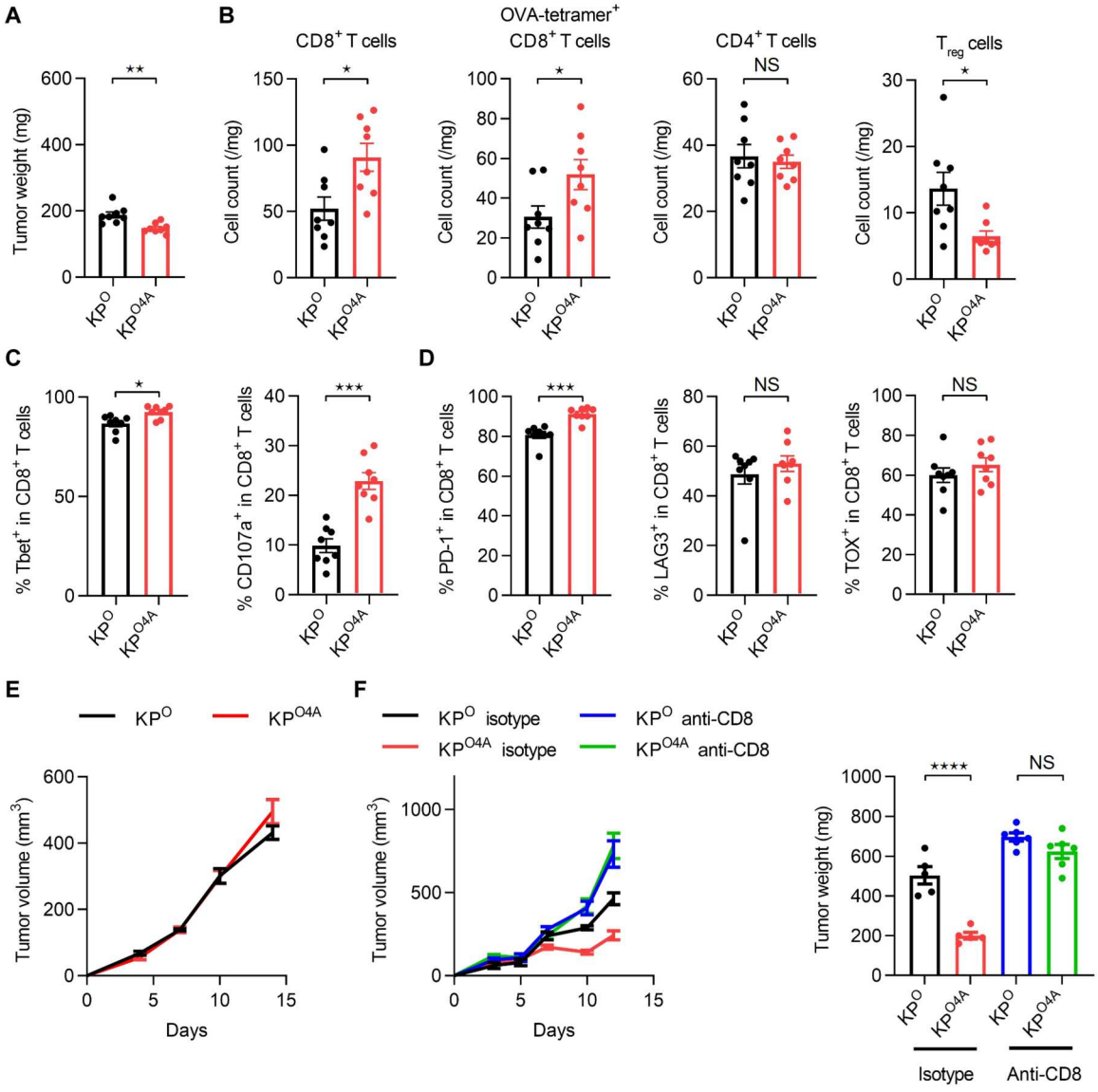

Fig. 3. Sema4A expression in LUAD cells improve antitumor immunity in murine models. (**A**) Tumor weight, (**B**) immune cell population profiling, (**C**) differentiation and activation, and (**D**) exhaustion markers of tumor-infiltrating lymphocytes (TILs) in $KP^{OVA\text{-}mock}$ (KP^{O}) versus $KP^{OVA\text{-}Sema4A}$ (KP^{O4A}) at day 8 after injection were analyzed by flow cytometry. $n = 8$ per group, NS, not significant, $^{*}P < 0.05$, $^{**}P < 0.01$, $^{***}P < 0.001$, Student's t test. (**E**) Tumor growth curves of mice subcutaneously injected with KP^{O} or KP^{O4A} cells (3×10^6 cells) in *Rag2* KO mice. $n = 5$ per group. (**F**) Tumor growth curves and tumor weight of mice subcutaneously injected with KP^{O} or KP^{O4A} cells (3×10^6 cells) and treated with anti-CD8 depletion antibody (Anti-CD8) or isotype control. $n = 5$ or 6 per group, $^{****}P < 0.0001$, one-way ANOVA. The experiments were performed at least three times with similar results. Results are expressed as the mean ± SEM.

Sema4A activates mTORC1 in T cells via plexin B and enhances S6K phosphorylation and the polyamine synthesis pathway

Because we found that rSema4A was able to enhance TCR stimulation, we investigated whether cell-extrinsic Sema4A stimulation could promote an antitumor effect through other immune cells. We confirmed that rSema4A bound to each immune cell population (fig. S14, A, C, and E) and that NK cells, GM-DCs, and FL-DCs did not exhibit activation or differentiation after rSema4A treatment (fig. S14, B, D, and F).

We then performed flow cytometry to assess rSema4A binding to tumor-infiltrating T cells. The binding of rSema4A to $CD8^+$ T cells in tumors was stronger than that to $CD4^+$ T cells (Fig. 5A). Plexin B1 and B2, which interact with Sema4A, were expressed in tumor-infiltrating $CD8^+$ T cells, whereas Neuropilin-1, which has also been reported to recognize Sema4A, was barely expressed in $CD8^+$ T cells in tumors (Fig. 5B). Therefore, plexinB1/B2 receptors are considered to play a major role in recognizing Sema4A in the TME. We also analyzed downstream signaling in $CD8^+$ T cells from $KP^{OVA\text{-}mock}$ and $KP^{OVA\text{-}Sema4A}$ tumors and found that phospho-p70 S6K was significantly increased in $CD8^+$ T cells from $KP^{OVA\text{-}Sema4A}$ tumors compared to $KP^{OVA\text{-}mock}$ tumors, whereas phospho-AKT (pAKT) (Ser^{473}) was significantly decreased, and pAKT (Thr^{308}) was comparable (Fig. 5C). These

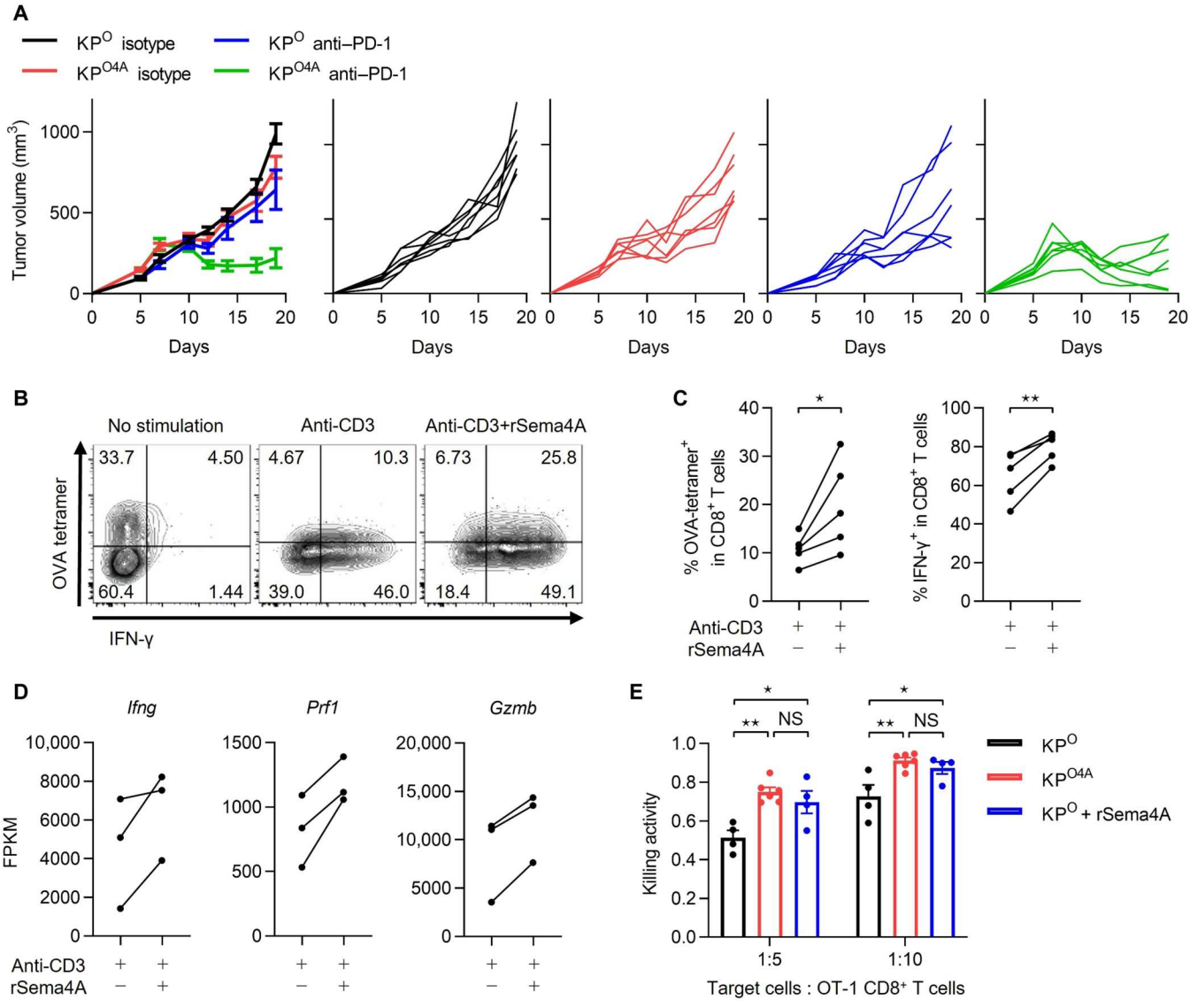

Fig. 4. rSema4A increases the sensitivity to antiPD-1 antibody treatment and the cytotoxic activity of CD8$^+$ T cells. – (**A**) Tumor growth curves in the subcutaneous tumor model. Anti–PD-1 antibody or isotype control were injected into mice, and therapeutic effects of KP$^{OVA\text{-}mock}$ (KP^O) and KP$^{OVA\text{-}Sema4A}$ (KP^{O4A}) were compared ($n = 7$ per group). The experiment was performed three times with similar results. (**B**) Representative flow cytometry data of the frequency of OVA-tetramer$^+$ and IFN-γ production in CD8$^+$ T cells from TILs. T cells from TILs were cultured with no stimulation, anti-CD3 antibody, and both anti-CD3 antibody and rSema4A. (**C**) Percentage of OVA-tetramer$^+$ and IFN-γ$^+$ in CD8$^+$ T cells after anti-CD3 antibody stimulation versus anti-CD3 antibody and rSema4A stimulation. $n = 5$ per group, $^*P < 0.05$, $^{**}P < 0.01$, paired t test. The experiment was performed three times with similar results. (**D**) mRNA expression of *Ifng*, *Prf1*, and *Gzmb* in CD8$^+$ T cells was compared after anti-CD3 antibody stimulation and anti-CD3 antibody plus rSema4A stimulation ($n = 3$). (**E**) Killing rate of cancer cells: KP^O and KP^{O4A} cells with OT-1 CD8$^+$ T cells. $n = 4$ to 6 per group, $^*P < 0.05$, $^{**}P < 0.01$, one-way ANOVA. The experiment was performed three times with similar results. Results are expressed as the mean ± SEM.

results suggest that in CD8$^+$ T cells, tumor-derived Sema4A induced a shift from mTORC2 to mTORC1 rather than to the phosphatidylinositol 3-kinase 3-phosphoinositide-dependent protein kinase 1 phospho-Akt(PI3K-PDK1-pAKT) (Thr^{308}) pathway, which is downstream of CD28, thus leading to reduced expression of pAKT (Ser^{473}).

Accordingly, rapamycin treatment canceled the tumor-specific T cell proliferation and activation induced by rSema4A (Fig. 5D). To further explore how Sema4A enhances the proliferation of CD8$^+$ T cells without inducing exhaustion, we evaluated RNA sequence data from tumor-infiltrating lymphocytes (TILs) stimulated with anti-CD3 antibodies and rSema4A and found that the following polyamine biosynthesis pathway-related transcriptomes were up-regulated in rSema4A-treated cells: *adenosylmethionine decarboxylase 1* (*Amd1*), *ornithine decarboxylase 1* (*Odc1*), and *spermidine synthase* (*Srm*) (Fig. 6A). The enhancement of the polyamine synthesis pathway by rSema4A significantly increased the levels of metabolites such as spermine and spermidine as measured by mass spectrometry (Fig. 6B). Regarding other metabolites, which we investigated by mass spectrometry, most amino acids showed no significant changes except for alanine, arginine, and aspartic acid (fig.

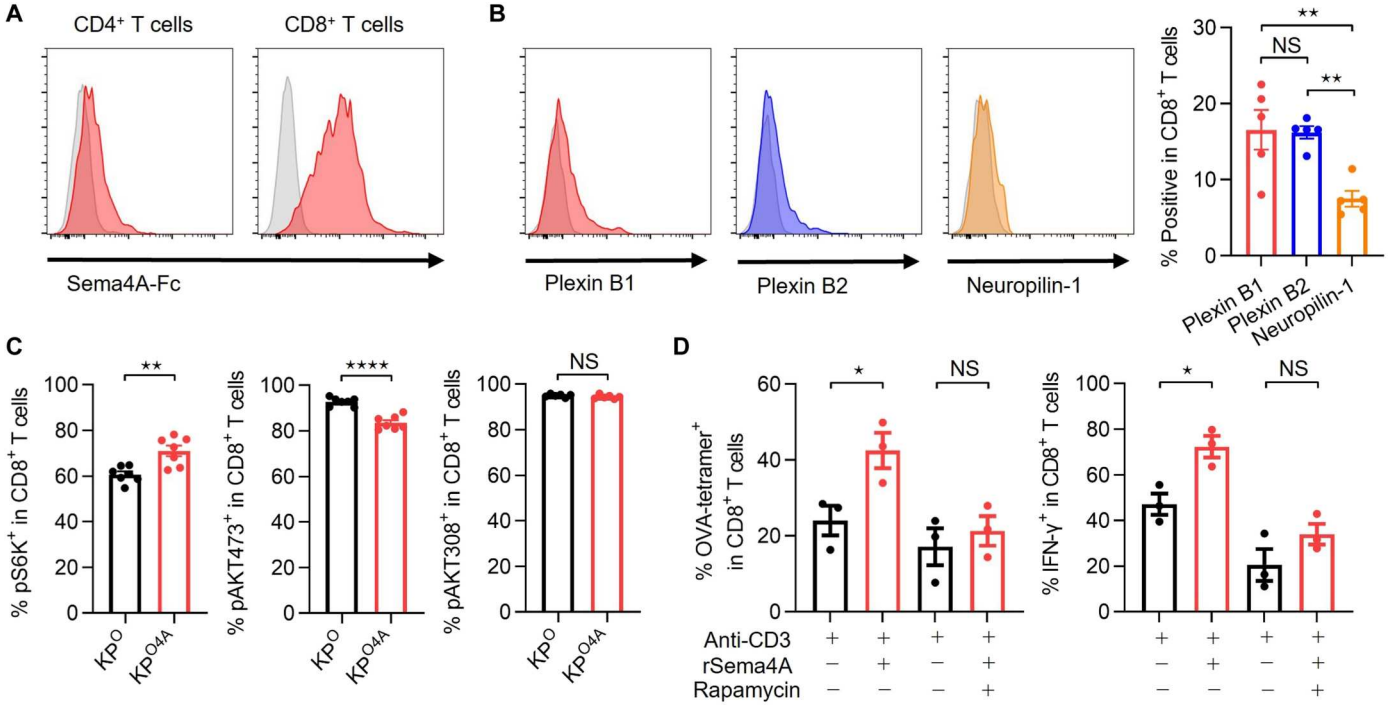

Fig. 5. The Sema4A–plexin B axis promotes CD8$^+$ T cell effector function by activating the mTOR-S6K signaling pathway. (**A**) CD4$^+$ T cells and CD8$^+$ T cells from TILs of KP$^{OVA\text{-}mock}$ (KP^O) tumors were incubated with Sema4A-Fc or control human IgG1 (hIgG). After washing, the amount of Sema4A-Fc binding to the cell surface was evaluated by flow cytometry using secondary antibody. The experiment was performed three times with similar results. (**B**) The expression levels and positivity of Sema4A receptors (plexin B1, plexin B2, and Neuropilin-1) in CD8$^+$ T cells were evaluated by flow cytometry. Cells were also stained with an isotype-matched control Ab (gray-filled histogram). $n = 5$ per group, $^{**}P < 0.01$, one-way ANOVA. The experiment was performed three times with similar results. (**C**) Intracellular phosphorylation levels of S6K, AKT (Ser^{473}), and AKT (Thr^{308}) were determined by intracellular staining. The positive rates in CD8$^+$ T cells were compared between KP^O and KP$^{OVA\text{-}Sema4A}$ (KP^{O4A}). $n = 7$ per group, $^{**}P < 0.01$, $^{****}P < 0.0001$, Student's t test. The experiment was performed three times with similar results. (**D**) Percentage of OVA-tetramer$^+$ and IFN-γ$^+$ CD8$^+$ T cells were compared after anti-CD3 antibody stimulation versus anti-CD3 antibody plus rSema4A stimulation, with or without rapamycin (20 ng/ml). $n = 3$ per group, $^*P < 0.05$, one-way ANOVA. The experiment was performed three times with similar results. Results are expressed as the mean ± SEM.

S15A). There were no significant differences in the three fatty acids analyzed (fig. S15B).

When TILs were treated with AMD-1 inhibitor (sardomozide dihydrochloride) and ODC-1 inhibitor (eflornithine hydrochloride hydrate), IFN-γ production was similarly up-regulated in rSema4A-treated cells compared to untreated cells. By contrast, Ki-67 expression showed no difference between CD8$^+$ T cells stimulated with anti-CD3 alone versus anti-CD3 plus rSema4A (Fig. 6C). These findings suggest that Sema4A activates mTORC1 in T cells and the polyamine biosynthesis pathway might be involved, particularly in the proliferation of T cells treated with rSema4A.

Administration of rSema4A improves the sensitivity to PD-1–blocking treatment

The aforementioned results verified the therapeutic effect of rSemaA administration in murine models. As expected, rSema4A and anti–PD-1 treatment improved the therapeutic outcome compared to each monotherapy (Fig. 7, A and B). Also, the therapeutic effect was abolished by depletion of CD8$^+$ T cells (Fig. 7C). In vivo administration of rSema4A improved OVA-specific T cell proliferation and IFN-γ production, resulting in a nonsignificant decrease in T_{regs} (Fig. 7D). Last, we evaluated rSema4A-stimulated tumor-infiltrating CD8$^+$ T cells from surgically resected human NSCLC and HNSCC tumors and from pleural effusion samples of patients with NSCLC. As with TILs in murine models, CD8$^+$ TILs treated with rSema4A showed elevated expression of IFN-γ and Ki-67 (Fig. 8, A and B). Together, these results demonstrate that Sema4A expressed by tumor cells was more effective than that expressed by immune cells in terms of ameliorating antitumor function and proliferation of CD8$^+$ T cells by promoting mTORC1-S6K signaling and polyamine synthesis (fig. S16).

DISCUSSION

This study demonstrated that tumor-infiltrating CD8$^+$ T cells were highly activated by Sema4A expressed in tumor cells in the TME, and this improved the sensitivity to PD-1–blocking treatment in both murine models and in patients with NSCLC. In our cohort, patients with Sema4A-positive NSCLCs showed a better therapeutic response to anti–PD-1 antibody than Sema4A-negative NSCLCs. Our analysis of a previously published scRNAseq dataset and mIHC of human NSCLC revealed that Sema4A expression was mainly detected on epithelial cells, including tumor cells in the TME of NSCLCs. This confirms that Sema4A expressed in tumor cells contributes significantly to activating cytotoxic CD8$^+$ T cells in the TME. GSEA using a TCGA dataset showed that high *SEMA4A* expression was significantly correlated with T cell activation and a favorable prognosis in patients with LUAD. Moreover,

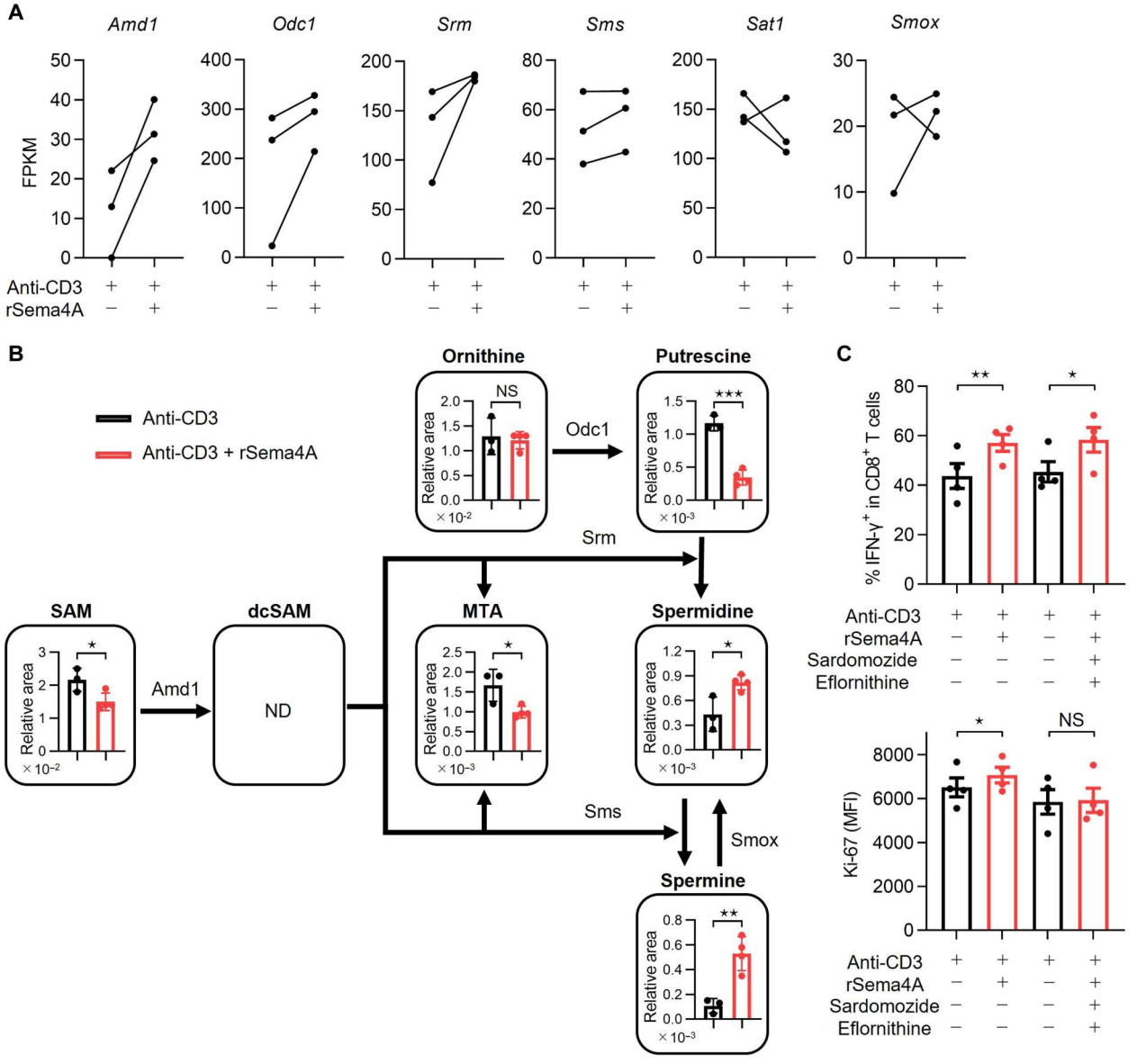

Fig. 6. The Sema4A–plexin B axis induces CD8$^+$ T cell proliferation by promoting the polyamine biosynthesis pathway. (**A**) mRNA expression levels of polyamine biosynthesis pathway components in CD8$^+$ T cells were compared after anti-CD3 antibody stimulation versus anti-CD3 antibody plus rSema4A stimulation (n = 3). (**B**) Summary of an analysis of metabolites involved in the polyamine biosynthesis pathway of CD8$^+$ T cells simulated with anti-CD3 antibody (n = 3) versus anti-CD3 antibody plus rSema4A stimulation (n = 4). ND, not detected, *P < 0.05, **P < 0.01, ***P < 0.001, Student's t test. (**C**) Percentage of IFN-γ$^+$ and mean fluorescence intensity (MFI) of Ki-67 in CD8$^+$ T cells after anti-CD3 antibody stimulation versus anti-CD3 antibody plus rSema4A stimulation with or without sardomozide dihydrochloride (10 μM) and eflornithine hydrochloride hydrate (500 μM). n = 3 per group, *P < 0.05, **P < 0.01, one-way ANOVA. SAM, S-adenosylmethionine; dcSAM, decarboxylated S-adenosylmethionine; MTA, methylthioadenosine. Results are expressed as the mean ± SEM.

the same trend was confirmed in patients with HNSCC and SKCM. Although we have previously shown that Sema4A expressed by DCs plays an important role in the activation and differentiation of CD4$^+$ T cells in mice (*19*, *20*), this study suggests that in terms of tumor-specific CD8$^+$ T cell activation, especially in patients with NSCLC, Sema4A can more efficiently function in the effector phase than in the priming phase because the dominant source of Sema4A is tumor cells in the TME.

Because the expression level of Sema4A was positively correlated with tumor growth inhibition and antigen-specific CD8$^+$ T cell infiltration in murine models, we explored how Sema4A on tumor cells enhanced CD8$^+$ T cell activity in the TME. rSema4A bound to tumor-infiltrating CD8$^+$ T cells much more strongly than to tumor-infiltrating CD4$^+$ T cells, suggesting that Sema4A mainly interacts with CD8$^+$ T cells in the TME. Although Sema4A particularly targets plexin B2 on CD8$^+$ T cells in murine infectious disease models (*34*), the expression of both plexin B1 and B2 was detected on CD8$^+$ T cells from TILs, suggesting that both plexins could be receptors for Sema4A in our cancer models. When isolated tumor-infiltrating CD8$^+$ T cells from patients with

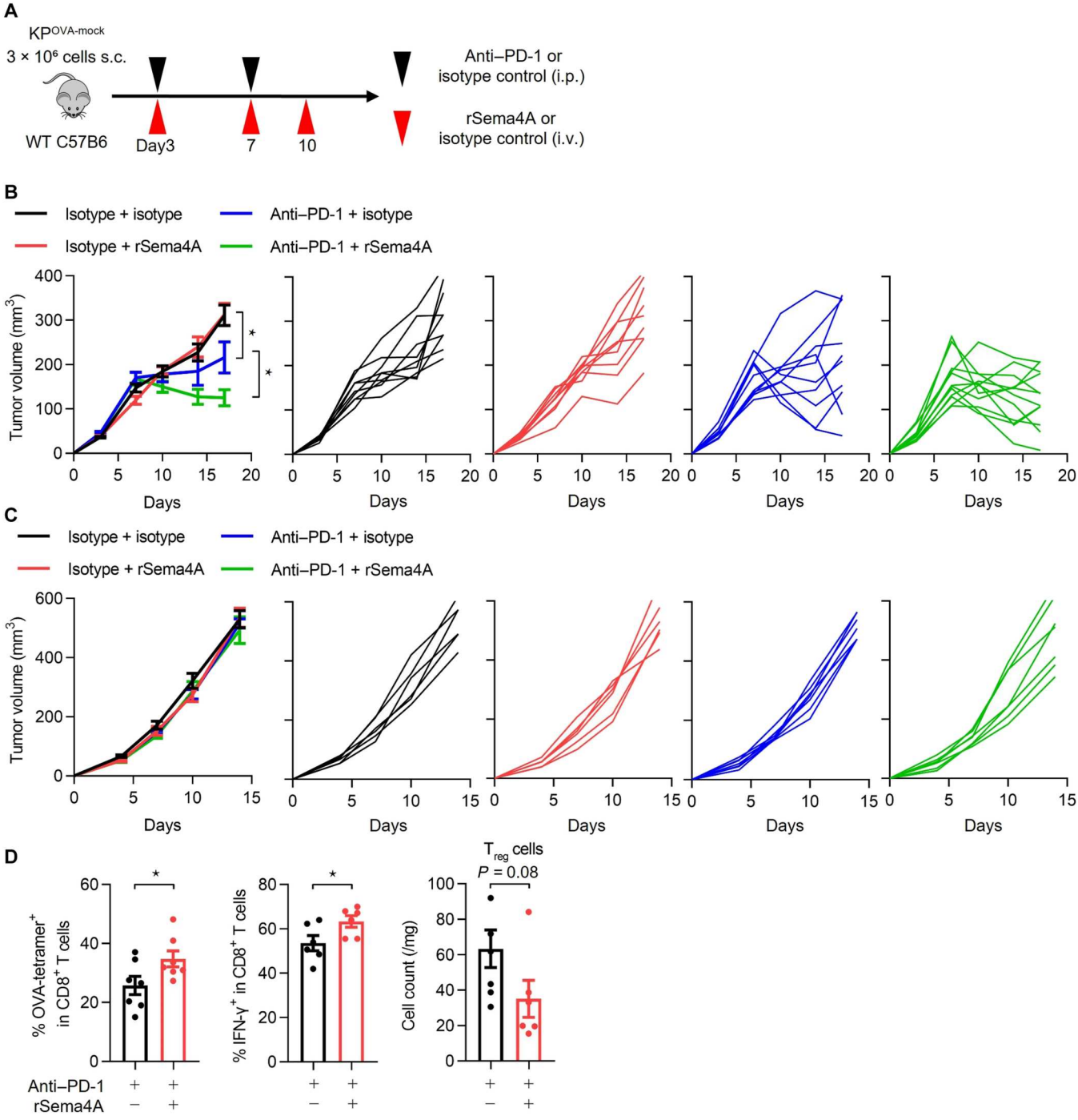

Fig. 7. rSema4A improves the efficacy of antiPD-1 antibody treatment in murine models. – (**A**) Schematic image of the treatment schedule in the subcutaneous tumor model. (**B**) Tumor growth curves of mice subcutaneously injected with $KP^{OVA\text{-}mock}$ cells (KP^{O}) (3×10^6 cells) and treated with anti–PD-1 antibodies or isotype control, with or without rSema4A. $n = 9$ to 12 per group, $^*P < 0.05$, one-way ANOVA. The experiment was performed three times with similar results. (**C**) Tumor growth curves of CD8-depleted mice subcutaneously injected with KP^{O} (3×10^6 cells) and treated with anti–PD-1 antibodies or isotype control, with or without rSema4A. $n = 6$ to 7 per group. The experiment was performed three times with similar results. (**D**) Percentage of OVA-tetramer$^+$ and IFN-γ$^+$ CD8$^+$ T cells and T_{reg} cell count from TILs were compared between the anti–PD-1 antibody group and the anti–PD-1 antibody plus rSema4A group. $n = 6$ to 7 per group, $^*P < 0.05$, Student's t test. The experiment was performed three times with similar results. Results are expressed as the mean ± SEM.

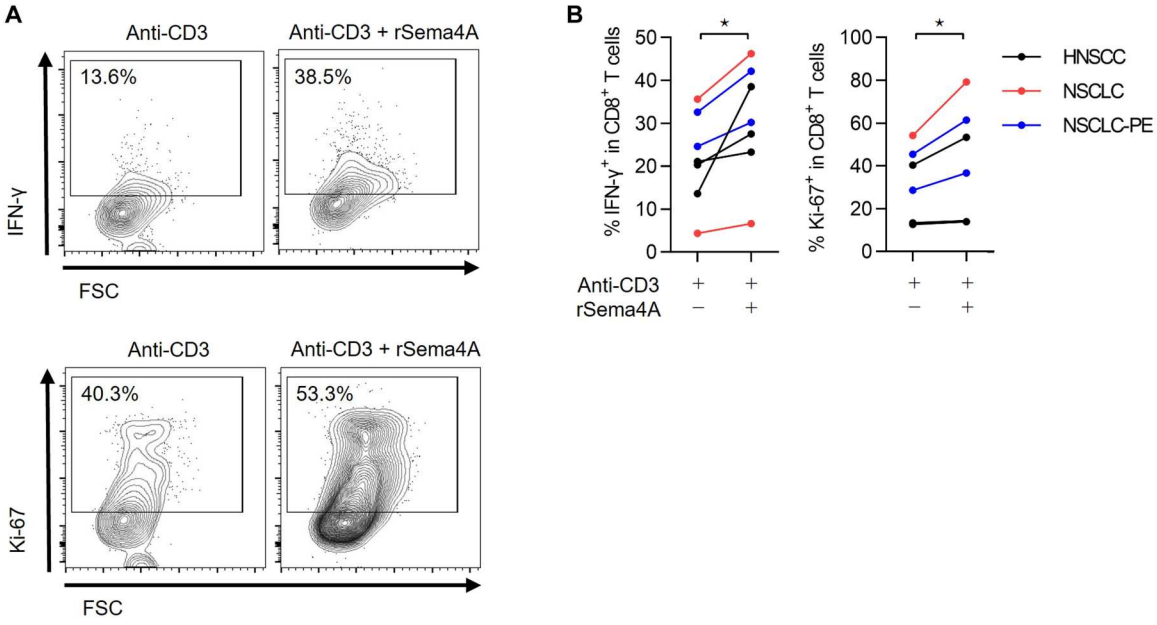

Fig. 8. rSema4A increases the effector function and proliferation of CD8$^+$ T cells from human tumors. (**A**) Representative flow cytometry data of the frequencies of IFN-γ production and Ki-67 positivity in CD8$^+$ T cells from TILs of human cancers. T cells from TILs were cultured with anti-CD3 antibody or both anti-CD3 antibody and rSema4A. FSC, forward scatter. (**B**) Percentages of CD8$^+$ T cells positive for IFN-γ ($n = 7$) and Ki-67 ($n = 5$) after anti-CD3 antibody stimulation versus anti-CD3 antibody plus rSema4A stimulation. *$P < 0.05$, paired t test. LC, lung cancer; LC-PE, pleural effusion of patients with lung cancer.

cancer were treated with rSema4A, the mTORC1-S6K pathway was up-regulated, which improves effector function by regulating Tbet and Eomes (*35*). In addition, we found that pAKT (Thr^{308}) expression showed no significant difference following stimulation with anti-CD3 antibody versus anti-CD3 antibody with rSema4A. These results suggest that Sema4A derived from tumors mainly induces a shift from mTORC2 to mTORC1, resulting in reduced expression of pAKT (Ser^{473}) without changing PI3K-PDK1-pAKT (Thr^{308}) signaling. This is consistent with the results of our previous report using an infection model (*34*) and another report focusing on the control of TOR partnering by semaphorin-plexin signaling in *Caenorhabditis elegans* (*36*).

A previous study demonstrated that mTORC1 activity was essential not only for the early differentiation of naïve T cells to effector T cells but also for the generation of effector responses induced by memory T cells (*37*). Sema4A may function mainly in the effector phase in the TME. Intriguingly, Sema4A stimulation increased tumor-specific CD8$^+$ T cell activation, but the treatment did not induce the terminal exhaustion markers LAG3 and TOX; rather, it improved proliferation in both murine models and in human tumor-infiltrating T cells. Recent studies demonstrated that stem-like memory T cells characterized by TCF1 expression augmented the therapeutic response to ICIs (*11*), whereas rSema4A stimulation did not alter the expression of stem-like markers, including TCF1, in CD8$^+$ T cells. These data suggest that CD8$^+$ T cell survival or proliferation could be modulated by additional mechanisms during rSema4A stimulation. As one possibility, we found that activation of mTORC1 by Sema4A promoted the polyamine synthesis pathway in CD8$^+$ T cells. Polyamines are small, polycationic molecules derived from L-arginine (*38*) and include putrescine, spermidine, and spermine in mammals. In polyamine synthesis, ODC converts ornithine to putrescine, and spermidine and spermine are synthesized by SRM and spermine synthase, respectively. SRM synthesis requires decarboxylated S-adenosylmethionine (dcSAM), which is converted from SAM by AMD-1. Previous studies showed that polyamine synthesis was required for T cell proliferation (*39*), and its inhibition suppressed their proliferation (*40*). AMD-1, a component of the polyamine synthesis pathway, has been reported to be enhanced by mTORC1 activation (*41*), which was consistent with our study. Among various amino acids, arginine was more significantly reduced following stimulation with anti-CD3 and rSema4A than with anti-CD3 alone. A recent paper reported that arginine is a major carbon donor for polyamine biosynthesis in T cells and that arginine consumption by T cells enhances polyamine synthesis and cell proliferation in vitro under low arginine concentrations (*42*). These results suggest that the tumor metabolic microenvironment accounted for a similar phenotype in our tumor model. On the other hand, the medium-chain fatty acid lauric acid (dodecanoic acid), which was recently reported to increase differentiation of T_H1 cells in CD4$^+$ T cells (*43*), did not show a significant difference between groups in our analysis. Accordingly, our data suggest that Sema4A could affect intracellular metabolism by modulating the polyamine synthesis pathway via mTORC1 activation and that it enhances the proliferative capacity of antigen-specific CD8$^+$ T cells. Further studies should clarify the mechanisms whereby Sema4a stimulation of T cells maintains cell proliferation and prevents exhaustion, including in the TME where nutritional conditions are poor.

In addition to the direct interaction between tumor-infiltrating CD8$^+$ T cells and Sema4A on tumor cells, immunosuppressive cells such as T_{regs} and G-MDSCs were reduced in Sema4A-expressing tumors, suggesting a possible role of Sema4A in optimizing the TME. Delgoffe *et al.* (*27*) reported that Sema4A stabilized T_{regs} through Neuropilin-1, and competitive inhibition of this pathway

by the Sema4A–immunoglobulin G (IgG) fusion protein destabilized T_{regs} in the TME, thus inhibiting tumor growth. These findings are consistent with the results of rSema4A administration in our study. rSema4A stimulates Sema4A/PlexinB signaling in $CD8^+$ T cells but inhibits Sema4A/ Neuropilin-1 signaling in T_{regs}. One reason for this may be that the Sema4A receptor differs between $CD8^+$ T cells and T_{regs}, although further investigation in the difference in both types of cells is warranted. We also performed combination treatment with rSema4A and anti–PD-1 antibody, which resulted in improved efficacy compared to anti–PD-1 antibody monotherapy, whereas rSema4A monotherapy had no therapeutic effect. T cell activation increases the expression of plexin B (*34*), and our data also indicated that rSema4A bound to $CD8^+$ T cells in the TME much more strongly than to splenic $CD8^+$ T cells in the same mice. These results suggest that even after systemic administration, rSema4A function, especially in the TME, might depend on the level of Sema4A-receptor expression by $CD8^+$ T cells, which would be reasonable because rSema4A acts as a T cell stimulator in the effector phase during T cell–tumor cell interaction. Future research will focus on the kinetics of systemic administration of rSema4A and improving its efficacy.

In summary, Sema4A promotes the effector function and proliferation of antigen-specific $CD8^+$ T cells in the TME in both mouse and human tumors. Sema4A expression in the TME could be vital biomarker to predict the response to ICIs. Moreover, inducing Sema4A expression in the TME might be a promising therapeutic strategy to improve ICI efficacy.

MATERIALS AND METHODS

Human study

All experimental protocols involving human specimens were approved by the Ethical Review Boards of the Graduate School of Medicine, Osaka University (nos. 752, 18528, and 843), the National Hospital Organization, Osaka Toneyama Medical Center (nos. 2018003 and 2018027), and the Osaka International Cancer Institute (no. 18207) and were carried out in accordance with the committee guidelines and regulations. The study was performed in accordance with the Declaration of Helsinki.

TCGA dataset analysis

The TCGA LUAD, HNSCC, and SKCM datasets were obtained from the UCSC Xenabrowser website (https://xenabrowser.net/): Prenormalized gene expression RNA sequencing data, phenotype information tables, and curated survival data tables were downloaded for each dataset and merged using the sample ID. Only samples with survival information were used for differential gene expression and GSEA. Furthermore, the LUAD and HNSCC datasets were subset to "Primary Tumor"–labeled samples only, while for SKCM, both "Primary Tumor" and "Metastatic" samples were used. Briefly, following the aforementioned filtering steps, samples were split into *SEMA4A*-high and *SEMA4A*-low groups using the median *SEMA4A* normalized expression value. Differential gene expression was carried out in R (version 4.0.4) using the DESeq2 package, and the test statistic column of the DESeq2 output was used to generate a ranked gene list that was in turn used as an input to the GSEA software, run in preranked mode, to identify enriched pathways from the Biological Process ontology (GO: BP) gene list of the MSigDB database (www.gsea-msigdb.org/gsea/msigdb/collections.jsp). Regarding survival analysis, the same *SEMA4A* threshold was used to split patients into *SEMA4A*-high and *SEMA4A*-low groups, and survival data were exported to GraphPad Prism for Kaplan-Meier curve plotting and null hypothesis testing.

Evaluation of the fraction of cells expressing *SEMA4A*

Lung cancer (LUAD) and normal lung tissue scRNAseq data was obtained from NCBI GEO (GSE131907) (*24*). RNA read counts and metadata were analyzed in R (version 4.0.4) using Seurat (version 4.0.5). The Seurat Object was set to select only the tLung Sample_Origin samples. The prefiltered and normalized data were scaled using the same settings as Kim *et al.* (*24*) (do.scale = FALSE, do.center = TRUE, scale.max = 10). Cell types were reclassified into groups using the provided "Cell_type" and "Cell_subtype" metadata to separate the T lymphocytes into $CD4^+$ and $CD8^+$ T cells, and the myeloid cells into DCs, macrophages, and monocytes. Otherwise, the original "Cell_type" classification was utilized. Cells with an "Undetermined" cell subtype as identified by the original authors were removed from the dataset. The fraction of *SEMA4A*-expressing cells was found by counting the number of cells expressing *SEMA4A* (defined as a *SEMA4A* relative expression level > 0) and dividing by the total number of cells for each cell type. That calculation was performed for each donor sample (n = 11).

IHC staining and image analysis

Formalin-fixed paraffin-embedded specimens obtained from surgical resections or transbronchial lung biopsy of NSCLCs were utilized for IHC assessment. Sema4A expression was examined with the primary rabbit anti-Sema4A polyclonal antibody (dilution 1:500, GeneTex), which was used in a previous study (*18*). After deparaffinization with xylene and rehydration with ethanol treatment, sections were heated to 125°C in target retrieval solution (Dako). After cooling, the sections were washed in tris-buffered saline with Tween 20, blocked with blocking solution (Dako) and normal goat serum (Vector Laboratories), and then incubated with anti-Sema4A antibody at 4°C overnight. Next, the sections were treated with Dako EnVision + System-HRP-Labeled Polymer Anti-Rabbit (Dako). Diaminobenzidine (Dako) was used as a chromogen. Sections were counterstained with hematoxylin and observed by microscopy. For each sample, two researchers (Y.Nai. and S.K.) and one pathologist (S.N.) independently categorized Sema4A expression as positive or negative. A level of ≥1% Sema4A expression in a tumor was defined as Sema4A positive, while a level of < 1% Sema4A expression was defined as Sema4A negative. Any inconsistencies between researchers in the evaluation process were subject to further adjudication. CD8 and granzyme B staining of mouse tumors from both the transgenic and subcutaneous models was performed by the Applied Medical Research Laboratory (Osaka, Japan). $CD8^+$ cells and granzyme B^+ cells were manually counted in at least three defined regions per sample: 1-mm^2 regions in the syngeneic model and nodules of similar size in the transgenic model. For mIHC, all slides were deparaffinized by baking for 30 min at 60°C in an incubator and then placed in xylene. Rehydration was performed using 99.5% ethanol. Antigen retrieval was performed in Target Retrieval Solution, pH9 (Dako) in a microwave oven until boiling, then in a steamer for 21 min at 100°C. Tissue sections were blocked with 0.3% hydrogen peroxide in miliQ for 15 min and then incubated with anti-CD11c antibody

for 30 min. The antibody was detected using the Opal Polymer HRP Ms + Rb (Onestep) (AKOYA Biosciences) detection system, before visualization using Opal520 TSA for another 10 min. Subsequently, antigen retrieval was conducted again in 10X Citrate Buffer, pH 6 (Sigma-Aldrich) to prepare the slides for the next antibody. Antibodies were diluted in Antibody Diluent (DAKO). Using this method, all samples were stained sequentially with the following: CD68 visualized with Opal570 TSA; SEMA4A visualized with Opal650 TSA; and pan-keratin visualized with Opal690 TSA. Slides were counterstained with 10X Spectral DAPI (Akoya Bioscience) for nuclear visualization for 10 min and coverslipped using ProLong Diamond Antifade Mountant (Invitrogen). All IHC slides were scanned using the Vectra 3.0.7, and images were visualized in Phenochart v.1.1 (AKOYA Bioscience). For immunofluorescence analysis, whole-slide images were scanned with five standard epifluorescence filters [4′,6-diamidino-2-phenylindole (DAPI), fluorescein isothiocyanate, Cy3, Texas Red, and Cy5]. A spectral library for each fluorophore was generated with inForm v2.5.1 (AKOYA Biosciences) using snapshots of representative tissue areas from slides stained for each fluorophore without DAPI staining. All images were spectrally unmixed using spectral libraries, and were analyzed in HALO v3.4 (Indica Labs).

Mouse study

All mice were maintained in specific pathogen–free conditions at the Institute of Experimental Animal Sciences, Osaka University. C57BL/6 J and BALB/c mice were purchased from CLEA Japan, and Lox-Stop-Lox-KrasG12D (B6.129S4-Krastm4Tyj/J) mice was purchased from The Jackson Laboratories (ME, USA). *Rag2* KO (*44*) was provided by the RIKEN BRC through the National BioResource Project of the MEXT, Japan. OVA-specific TCR OT-1 transgenic mice were used on a C57BL/6 J background and C57BL/6 J Sema4A-deficient mice were generated as previously described. Adenovirus-carrying Cre recombinase (5×10^6 titer) (University of Iowa) was administered intranasally at 6 weeks of age to induce tumors in Lox-Stop-Lox-KrasG12D mice (*30*). All breeding and in vivo experiments were performed in accordance with the Regulations on Animal Experiments at Osaka University.

Cell line establishment

Mouse lung cancer cell lines were established from lung tumor nodules from mice with mutated $Kras^{G12D}$ and homozygous *Tp53* deletion, as described previously (*30*), and are referred to as KP cell lines. These cell lines were grown in RPMI (Nacalai Tesque) supplemented with 10% fetal bovine serum (FBS), penicillin (100 U/ml), and streptomycin (100 mg/ml). Mouse oral squamous cell carcinoma cell lines (MOC2) were purchased (Kerafast) and cultured according to the described culture conditions. WEHI-3B were purchased from the National Institutes of Biomedical Innovation, Health, and Nutrition, and cultured as described. OVA-expressing cells and Sema4A-expressing cells were generated using the pMX retroviral vector system, as previously described (*45*, *46*). In brief, the full OVA segment was amplified by polymerase chain reaction and cloned into a pMX retroviral vector at the Bam HI and Sal I restriction sites. The mouse Sema4A (*mSema4a*) coding region (NM_001163491) (ORIGENE) was synthesized with the 5′ Eco RI and 3′ Not I restriction site and then cloned into a pMX retroviral vector at the corresponding sites. Retroviral supernatants were generated by transfecting the retrovirus packaging vector and each pMX vector containing the gene of interest into the 293 T cell line. After transduction with polybrene (8 μg/ml), single cell–derived clones were obtained by limiting dilution. The expression of OVA was confirmed by IFN-γ production after coculture, with the splenocytes from an OT-1 mouse as an indicator. KP cell lines and KP-expressing and MOC2-expressing OVA (KP^{OVA} and $MOC2^{OVA}$) was transfected with retroviral vectors containing Sema4A (KP^{Sema4A}, $KP^{OVA\text{-}Sema4A}$, and $MOC2^{OVA\text{-}Sema4A}$). Expression of Sema4A in WEHI-3B cells was silenced by the lentiviral introduction of an shRNA targeting Sema4A (VB900060-6130vbt) or scramble control (VectorBuilder). The expression level of OVA and Sema4A was checked by flow cytometry. The sorting of low and high Sema4A-expressing cells that express comparable levels of OVA was performed using a BD FACSAria II cell sorter (BD Biosciences).

NK cell killing assay

NK cells were isolated from splenocytes using a MojoSort Mouse NK cell isolation kit (BioLegend). The cytolytic activity of NK cells was tested against NK-sensitive (YAC-1) and KP9-3 cells in a ^{51}Cr release assay. Tumor cell lines were labeled with ^{51}Cr by incubating 1×10^4 cells in 0.5 μCi of ^{51}Cr for 1.5 hours at 37°C. Labeled cells were washed three times with phosphate-buffered saline (PBS) or resuspended in complete RPMI medium and plated in 96-well flat bottom plates (CORNING) in triplicate at a concentration of 2×10^5 cells/ml. Effector cells were added at the indicated effector:target ratios to plates incubated at 37°C for 4 hours. Supernatants were collected and the released ^{51}Cr was counted using a gamma counter. Cells were treated with 1% Triton X-100 or with water as a measure of maximal killing. Target cells incubated without effector cells were used to measure spontaneous ^{51}Cr release. Counts from triplicate wells were averaged, and then percent lysis was calculated using the following equation: % specific lysis = 100 × [(test ^{51}Cr release) − (spontaneous ^{51}Cr release)] / [(maximal ^{51}Cr release) − (spontaneous ^{51}Cr release)].

Generation of bone marrow–derived DCs

The tibias and femurs from WT mice were removed under sterile conditions. Both ends of the bone were cut off with scissors, and the bone marrow was rinsed out of the cavity into a sterile culture dish with 2% FBS in PBS. The cell suspension in the dish was collected and centrifuged, and the supernatant was discarded. The cell pellet was resuspended with red blood cell (RBC) lysis buffer. Following the second centrifugation, the supernatant was discarded, and the pelleted cells were washed with 2% FBS in PBS and collected. GM-DCs were generated by culturing bone marrow cells with GM-CSF (20 ng/ml; R&D Systems) in complete RPMI for 6 to 8 days as previously described (*47*). For FL-DCs, Flt3L (200 ng/ml; PeproTech) was used instead of GM-CSF.

OT-1 $CD8^+$ T cell proliferation assay

$CD8^+$ T cells from splenocytes of OT-1 TCR-Tg mice were isolated using a MojoSort Mouse CD8 T cell isolation kit (BioLegend), and stained with 0.5 μM carboxyfluorescein succinimidyl ester (CFSE) (Thermo Fisher Scientific Inc., Waltham, MA, USA). For the in vitro assay, these cells were cocultured with different concentrations of GM-DCs or TAMs in a round-bottom 96-well plate in the presence of OVA peptides (10 μg/ml; Sigma) were recognized by OT-1 lymphocytes. After a 72-hour incubation, the cells were stained with

antibodies for the T cell markers. Flow cytometry was used to analyze the CFSE dilution that occurred with each cell division.

Cancer cell stimulation and proliferation assay

Cancer cell lines were cultured in RPMI (Nacalai Tesque) supplemented with 10% FBS, penicillin (100 U/ml), streptomycin (100 mg/ml), and mIFN-γ (20 ng/ml; R&D Systems) for 24 hours to investigate the expression of H2Kb SIINFEKL. Cell proliferation ability was measured using a Cell Counting Kit-8 (DOJONDO).

Immune cell isolation from murine tumor samples and analysis

Tumor-bearing mice were euthanized, and resected tumors were shredded into small pieces and incubated in collagenase-containing buffer: collagenase type IV (100 U/ml; Invitrogen), deoxyribonuclease I (50 μg/ml; Roche), and 10% FBS in RPMI 1640 medium for 45 min. After incubation, cells were treated with RBC lysis buffer (Thermo Fisher Scientific) and passed through a 100-μm cell strainer to remove debris. The cell pellet was dissolved by 2% FBS in PBS and used for flow cytometry analysis. Isolated cells were initially stained with the LIVE/DEAD Fixable Dead Cell Stain Kit (Invitrogen). Cells were subsequently incubated with Fc-blocking antibody (BioLegend) and then stained with monoclonal antibodies for several surface and intracellular antigens as listed in Supplementary Methods. Foxp3/Transcription Factor Staining Buffer (eBioscience) was used for intracellular staining. Sample acquisition was performed on a BD FACSCanto II cytometer (BD Biosciences) equipped with Diva software and analyzed using FlowJo software (BD Biosciences). Antibody clone numbers for immune analysis are listed in the Supplementary Materials.

TAM sorting

Immune-cell isolation was performed as above, and sorting of TAMs (living $CD45^+$ $F4/80^+$ cells) was performed using a BD FACSAria II cell sorter (BD Biosciences).

Mouse treatment studies

Mice were subcutaneously inoculated with 3×10^6 tumor cells for survival and treatment analysis and 5×10^6 tumor cells for immune profiling. Intravenous injection was performed with 2×10^5 tumor cells. Intratracheal inoculation was conducted as follows. Mice were anesthetized and supported on an intubation stand (Natsume). A 22-G catheter (TERUMO) was inserted into the trachea. A cell suspension containing 1×10^6 cells in 50-μl sterile PBS was pipetted into the catheter and inhaled by mice. For $CD8^+$ T cell depletion experiments, anti-CD8α (clone 53-6.7) (100 μg per mouse) (Bio X Cell) and isotype control antibody (rat IgG2a, Bio X Cell) (100 μg per mouse) were injected intraperitoneally at days −1, 3, 6, and 10 after tumor inoculation. For anti–PD-1 antibody treatment, anti–PD-1 antibody (clone RMP1–14) (200 μg per mouse) (Bio X Cell) and isotype control antibody (rat IgG2a, Bio X Cell) (200 μg per mouse) were intraperitoneally injected twice a week from day 3 to day 10. Recombinant mouse Sema4A-Fc (50 μg per mouse) was purchased from Oriental Yeast and intravenously injected at days 3, 7, and 10 after tumor inoculation. Tumor size was measured using calipers, and tumor volume was calculated using the following formula: (major axis × minor axis^2) × 0.5.

In vitro stimulation of $CD8^+$ T cells

Mononuclear cells were enriched from tumor suspensions by Ficoll-Paque (GE Healthcare). Cells were cultured in RPMI 1640 medium (Nacalai Tesque) supplemented with 10% FBS, penicillin (100 U/ml), and streptomycin (100 mg/ml). For in vitro stimulation of effector cells, $CD8^+$ T cells were stimulated for 2 days with plate-bound anti-CD3ε antibody (1 μg/ml, 2C11; BD Pharmingen) or plate-bound anti-CD3ε and recombinant mouse Sema4A-His (10 μg/ml, LSBio). In the experiment to investigate the IFN-γ–producing ability of T cells from the treatment study, cells were stimulated with Cell Stimulation Cocktail (eBioscience) according to the datasheet. In the inhibition experiments, rapamycin (25 ng/ml, Sigma), sardomozide dihydrochloride (10 μM, Medchemexpress), and eflornithine hydrochloride hydrate (500 μM, Medchemexpress) were added. For human samples, anti-CD3 antibody (5 μg/ml, OKT-3; BioLegend) and recombinant human Sema4A-His (10 μg/ml, Sinobiological) were used. Antibody clone numbers for immune analysis are listed in the Supplementary Materials.

In vitro stimulation of NK cells and DCs

NK cells were isolated from splenocytes, and DCs were generated from bone marrow as above. For in vitro stimulation, NK cells and DCs were stimulated for 24 hours with plate-bound recombinant mouse Sema4A-His (10 μg/ml, LSBio). NK cells were cultured in RPMI (Nacalai Tesque) supplemented with 10% FBS, penicillin (100 U/ml), streptomycin (100 mg/ml), and mouse Interleukin-2 (mIL-2) (100 U/ml, R&D Systems).

Tumor-infiltrating T cell sorting and RNA sequencing

Tumor-infiltrating $CD8^+$ T cells stimulated in vitro were prepared as above. After stimulation, sorting of activated antigen-specific T cells (living $CD45^+$ $CD8^+$ OVA-tetramer$^+$ cells) was performed using a BD FACSAria II cell sorter (BD Biosciences). Total RNA was extracted from cells with an miRNeasy Mini Kit (Qiagen) according to the manufacturer′s protocol. Full-length complementary DNA was generated using a SMART-Seq HT Kit (Takara Bio) according to the manufacturer′s instructions. An Illumina library was prepared using a Nextera DNA Library Preparation Kit (Illumina) according to the SMARTer kit instructions. Sequencing was performed on an Illumina NovaSeq 6000 sequencer (Illumina) in the 100-base single-end mode. Sequenced reads were mapped to the human reference genome sequence (hg19) using TopHat v2.0.12. Fragments per kilobase of exons per million mapped fragments were calculated using Cufflinks v2.1.1. Raw data were deposited in the NCBI′s GEO database (GEO GSE208167).

Cytotoxic T cell killing assay

Prior to the coculture assay, cancer cell lines (KP^{OVA} and $KP^{OVA\text{-}Sema4A}$) were stimulated with mIFN-γ (20 ng/ml; R&D Systems) overnight. $CD8^+$ T cells from splenocytes of OT-1 $Rag^{-/-}$ mice were isolated using a MojoSort Mouse CD8 T cell isolation kit (BioLegend). A total of 1×10^4 cancer cells were seeded in a flat-bottom 96-well plate and cocultured with different concentrations of $CD8^+$ T cells (1:0, 1:5, and 1:10) with or without recombinant mouse Sema4A-His (1 μg/ml, LSBio). After a 48-hour incubation, living cancer cells (alive $CD45^-$) were counted by flow cytometry. Killing activity was calculated using the following equation: killing activity = 100 × {1 − [(alive $CD45^-$

without T cells) − (alive CD45$^-$ treated with T cells)] / (alive CD45$^-$ without T cells)}.

rSema4A binding assay

To detect rSema4A binding, immune cells were incubated with rSema4A-Fc (10 μg/ml, Aipogen) for 30 min after dead cell staining and Fc blocking. Cells were washed with 2% FBS in PBS and incubated with anti-human IgG1-R-phycoerythrin (5 μg/ml, Southern Biotech) for 30 min as secondary antibody. Binding of rSema4A was detected by flow cytometry.

Metabolite extraction

CD8$^+$ T cells from splenocytes of tumor-bearing WT mice stimulated in vitro were prepared as above. After stimulation, sorting of CD8$^+$ T cells (living CD45$^+$ CD8$^+$ cells) was performed using a BD FACSAria II cell sorter (BD Biosciences). The cell suspension was transferred to a tube and centrifuged to pellet the cells. Culture medium was aspirated from the tube, and the cells were washed with 10 ml of 5% mannitol solution. The cells were then treated with 800 μl of methanol and vortexed for 30 s to suppress enzymatic activity. Next, 550 μl of Milli-Q water containing internal standards [H3304-1002, Human Metabolome Technologies Inc. (HMT), Yamagata, Japan] was added to the cell extract, which was vortexed for another 30 s. The extract was then centrifuged at 2300*g* at 4°C for 5 min, after which 700 μl of the supernatant was centrifugally filtered through a Millipore 5-kDa cutoff filter (UltrafreeMC-PLHCC, HMT) at 9100*g* at 4°C for 120 min to remove macromolecules. Subsequently, the filtrate was evaporated to dryness under a vacuum and reconstituted in 50 μl of Milli-Q water for metabolome analysis at HMT.

Metabolome analysis (ω scan)

Metabolome analysis was conducted according to HMT's ω Scan package, using capillary electrophoresis Fourier transform mass spectrometry (CE-FTMS) based on the methods described previously (*48*). Briefly, CE-FTMS analysis was carried out using an Agilent 7100 CE capillary electrophoresis system equipped with a Q Exactive Plus (Thermo Fisher Scientific), an Agilent 1260 isocratic HPLC pump, an Agilent G1603A CE-MS adapter kit, and an Agilent G1607A CE-ESI-MS sprayer kit (Agilent Technologies Inc., Santa Clara, CA, USA). The systems were controlled by Agilent MassHunter workstation software LC/MS data acquisition for 6200 series TOF/6500 series Q-TOF version B.08.00 (Agilent Technologies) and Xcalibur (Thermo Fisher Scientific) and connected by a fused silica capillary (50-μm inner diameter by 80-cm total length) with commercial electrophoresis buffer (H3301-1001 and I3302-1023 for cation and anion analyses, respectively, HMT) as the electrolyte. The spectrometer was scanned from mass/charge ratio (*m*/*z*) 50 to 1000 in positive mode and from *m*/*z* 70 to 1050 in negative mode. Peaks were extracted using MasterHands (Keio University, Yamagata, Japan), an automatic integration software system, to obtain peak information including *m*/*z*, peak area, and migration time (MT) (*49*). Signal peaks corresponding to isotopomers, adduct ions, and other product ions of known metabolites were excluded, and the remaining peaks were annotated according to HMT's metabolite database based on their *m*/*z* values and MTs. Areas of the annotated peaks were then normalized to internal standards and sample volume to obtain relative levels of each metabolite. Hierarchical cluster analysis and principal components analysis (*50*) were performed by HMT's proprietary MATLAB and R programs, respectively. Detected metabolites were plotted on metabolic pathway maps using VANTED software (*51*).

Immune cell isolation from human samples

Surgically resected fresh tumors from patients with NSCLC or HNSCC were shredded into small pieces and transferred into a gentleMACS C tube (Miltenyi Biotec) that contained the reagents of a tumor dissociation kit (Miltenyi Biotec). Minced tumors were dissociated gently with a gentleMACS dissociator (Miltenyi Biotec) to yield cell suspensions. Next, cells were treated with RBC lysis buffer, and the debris was removed as described above. Pleural effusion fluid from patients with lung cancer was treated in the same way.

Statistical analysis

All statistical analyses were performed in GraphPad Prism 7. Survival analysis was performed using Kaplan-Meier survival plots, and the log-rank test *P* value was calculated. Patients' survival data were censored at 5 years. Student's *t* test and the paired *t* test were used for two-group comparisons, while one-way analysis of variance (ANOVA) was used for comparisons of more than two groups. Fisher's exact test was used to compare two categorical variables. Numerical data are presented as means ± SEM. A *P* value of less than 0.05 was considered significant.

Supplementary Materials

This PDF file includes:

Figs. S1 to S16
Tables S1 to S5

View/request a protocol for this paper from *Bio-protocol*.

REFERENCES AND NOTES

1. G. G. Lagos, B. Izar, N. A. Rizvi, Beyond tumor PD-L1: Emerging genomic biomarkers for checkpoint inhibitor immunotherapy. *Am. Soc. Clin. Oncol. Educ. Book* **40**, 1–11 (2020).
2. S. H. Baumeister, G. J. Freeman, G. Dranoff, A. H. Sharpe, Coinhibitory pathways in immunotherapy for cancer. *Annu. Rev. Immunol.* **34**, 539–573 (2016).
3. Y. Choi, Y. Shi, C. L. Haymaker, A. Naing, G. Ciliberto, J. Hajjar, T-cell agonists in cancer immunotherapy. *J. Immunother. Cancer* **8**, e000966 (2020).
4. P. Chongsathidkiet, C. Jackson, S. Koyama, F. Loebel, X. Cui, S. H. Farber, K. Woroniecka, A. A. Elsamadicy, C. A. Dechant, H. R. Kemeny, L. Sanchez-Perez, T. A. Cheema, N. C. Souders, J. E. Herndon, J. V. Coumans, J. I. Everitt, B. V. Nahed, J. H. Sampson, M. D. Gunn, R. L. Martuza, G. Dranoff, W. T. Curry, P. E. Fecci, Sequestration of T cells in bone marrow in the setting of glioblastoma and other intracranial tumors. *Nat. Med.* **24**, 1459–1468 (2018).
5. V. Vezys, P. Penaloza-MacMaster, D. L. Barber, S. J. Ha, B. Konieczny, G. J. Freeman, R. S. Mittler, R. Ahmed, 4-1BB signaling synergizes with programmed death ligand 1 blockade to augment CD8 T cell responses during chronic viral infection. *J. Immunol.* **187**, 1634–1642 (2011).
6. S. Buchan, T. Manzo, B. Flutter, A. Rogel, N. Edwards, L. Zhang, S. Sivakumaran, S. Ghorashian, B. Carpenter, C. Bennett, G. J. Freeman, M. Sykes, M. Croft, A. Al-Shamkhani, R. Chakraverty, OX40- and CD27-mediated costimulation synergizes with anti-PD-L1 blockade by forcing exhausted CD8$^+$ T cells to exit quiescence. *J. Immunol.* **194**, 125–133 (2015).
7. D. S. Thommen, V. H. Koelzer, P. Herzig, A. Roller, M. Trefny, S. Dimeloe, A. Kiialainen, J. Hanhart, C. Schill, C. Hess, S. Savic Prince, M. Wiese, D. Lardinois, P. C. Ho, C. Klein, V. Karanikas, K. D. Mertz, T. N. Schumacher, A. Zippelius, A transcriptionally and functionally distinct PD-1$^+$ CD8$^+$ T cell pool with predictive potential in non-small-cell lung cancer treated with PD-1 blockade. *Nat. Med.* **24**, 994–1004 (2018).
8. C. U. Blank, W. N. Haining, W. Held, P. G. Hogan, A. Kallies, E. Lugli, R. C. Lynn, M. Philip, A. Rao, N. P. Restifo, A. Schietinger, T. N. Schumacher, P. L. Schwartzberg, A. H. Sharpe, D. E. Speiser, E. J. Wherry, B. A. Youngblood, D. Zehn, Defining 'T cell exhaustion'. *Nat. Rev. Immunol.* **19**, 665–674 (2019).

9. J. C. Beltra, S. Manne, M. S. Abdel-Hakeem, M. Kurachi, J. R. Giles, Z. Chen, V. Casella, S. F. Ngiow, O. Khan, Y. J. Huang, P. Yan, K. Nzingha, W. Xu, R. K. Amaravadi, X. Xu, G. C. Karakousis, T. C. Mitchell, L. M. Schuchter, A. C. Huang, E. J. Wherry, Developmental relationships of four exhausted $CD8^+$ T cell subsets reveals underlying transcriptional and epigenetic landscape control mechanisms. *Immunity* **52**, 825–841.e8 (2020).
10. B. C. Miller, D. R. Sen, R. Al Abosy, K. Bi, Y. V. Virkud, M. W. LaFleur, K. B. Yates, A. Lako, K. Felt, G. S. Naik, M. Manos, E. Gjini, J. R. Kuchroo, J. J. Ishizuka, J. L. Collier, G. K. Griffin, S. Maleri, D. E. Comstock, S. A. Weiss, F. D. Brown, A. Panda, M. D. Zimmer, R. T. Manguso, F. S. Hodi, S. J. Rodig, A. H. Sharpe, W. N. Haining, Subsets of exhausted $CD8^+$ T cells differentially mediate tumor control and respond to checkpoint blockade. *Nat. Immunol.* **20**, 326–336 (2019).
11. I. Siddiqui, K. Schaeuble, V. Chennupati, S. A. Fuertes Marraco, S. Calderon-Copete, D. Pais Ferreira, S. J. Carmona, L. Scarpellino, D. Gfeller, S. Pradervand, S. A. Luther, D. E. Speiser, W. Held, Intratumoral $Tcf1^+PD\text{-}1^+CD8^+$ T cells with stem-like properties promote tumor control in response to vaccination and checkpoint blockade immunotherapy. *Immunity* **50**, 195–211.e10 (2019).
12. J. A. Shyer, R. A. Flavell, W. Bailis, Metabolic signaling in T cells. *Cell Res.* **30**, 649–659 (2020).
13. K. N. Pollizzi, I. H. Sun, C. H. Patel, Y. C. Lo, M. H. Oh, A. T. Waickman, A. J. Tam, R. L. Blosser, J. Wen, G. M. Delgoffe, J. D. Powell, Asymmetric inheritance of mTORC1 kinase activity during division dictates $CD8^+$ T cell differentiation. *Nat. Immunol.* **17**, 704–711 (2016).
14. D. K. Finlay, E. Rosenzweig, L. V. Sinclair, C. Feijoo-Carnero, J. L. Hukelmann, J. Rolf, A. A. Panteleyev, K. Okkenhaug, D. A. Cantrell, PDK1 regulation of mTOR and hypoxia-inducible factor 1 integrate metabolism and migration of $CD8^+$ T cells. *J. Exp. Med.* **209**, 2441–2453 (2012).
15. H. Takamatsu, A. Kumanogoh, Diverse roles for semaphorin-plexin signaling in the immune system. *Trends Immunol.* **33**, 127–135 (2012).
16. R. Mastrantonio, H. You, L. Tamagnone, Semaphorins as emerging clinical biomarkers and therapeutic targets in cancer. *Theranostics* **11**, 3262–3277 (2021).
17. S. P. Chapoval, M. Hritzo, X. Qi, L. Tamagnone, A. Golding, A. D. Keegan, Semaphorin 4A stabilizes human regulatory T cell phenotype via plexin B1. *Immunohorizons* **3**, 71–87 (2019).
18. T. Sun, L. Yang, H. Kaur, J. Pestel, M. Looso, H. Nolte, C. Krasel, D. Heil, R. K. Krishnan, M. J. Santoni, J. P. Borg, M. Bunemann, S. Offermanns, J. M. Swiercz, T. Worzfeld, A reverse signaling pathway downstream of Sema4A controls cell migration via Scrib. *J. Cell Biol.* **216**, 199–215 (2017).
19. A. Kumanogoh, S. Marukawa, K. Suzuki, N. Takegahara, C. Watanabe, E. Ch'ng, I. Ishida, H. Fujimura, S. Sakoda, K. Yoshida, H. Kikutani, Class IV semaphorin Sema4A enhances T-cell activation and interacts with Tim-2. *Nature* **419**, 629–633 (2002).
20. A. Kumanogoh, T. Shikina, K. Suzuki, S. Uematsu, K. Yukawa, S. Kashiwamura, H. Tsutsui, M. Yamamoto, H. Takamatsu, E. P. Ko-Mitamura, N. Takegahara, S. Marukawa, I. Ishida, H. Morishita, D. V. Prasad, M. Tamura, M. Mizui, T. Toyofuku, S. Akira, K. Takeda, M. Okabe, H. Kikutani, Nonredundant roles of Sema4A in the immune system: Defective T cell priming and Th1/Th2 regulation in Sema4A-deficient mice. *Immunity* **22**, 305–316 (2005).
21. Y. Suga, I. Nagatomo, Y. Kinehara, S. Koyama, D. Okuzaki, A. Osa, Y. Naito, H. Takamatsu, M. Nishide, S. Nojima, D. Ito, T. Tsuda, T. Nakatani, Y. Nakanishi, Y. Futami, T. Koba, S. Satoh, Y. Hosono, K. Miyake, K. Fukushima, T. Shiroyama, K. Iwahori, H. Hirata, Y. Takeda, A. Kumanogoh, IL-33 induces Sema4A expression in dendritic cells and exerts antitumor immunity. *J. Immunol.* **207**, 1456–1467 (2021).
22. X. Q. Liu, Y. Yao, J. W. Mu, F. Y. Yang, Semaphorin 4A restricts tumor progression by inhibiting angiogenesis of oral squamous cell carcinoma cells. *Tissue Cell* **69**, 101485 (2021).
23. D. Ito, A. Kumanogoh, The role of Sema4A in angiogenesis, immune responses, carcinogenesis, and retinal systems. *Cell Adh. Migr.* **10**, 692–699 (2016).
24. N. Kim, H. K. Kim, K. Lee, Y. Hong, J. H. Cho, J. W. Choi, J. I. Lee, Y. L. Suh, B. M. Ku, H. H. Eum, S. Choi, Y. L. Choi, J. G. Joung, W. Y. Park, H. A. Jung, J. M. Sun, S. H. Lee, J. S. Ahn, K. Park, M. J. Ahn, H. O. Lee, Single-cell RNA sequencing demonstrates the molecular and cellular reprogramming of metastatic lung adenocarcinoma. *Nat. Commun.* **11**, 2285 (2020).
25. M. Rokavec, D. Horst, H. Hermeking, Cellular model of colon cancer progression reveals signatures of mRNAs, miRNA, lncRNAs, and epigenetic modifications associated with metastasis. *Cancer Res.* **77**, 1854–1867 (2017).
26. A. S. Iyer, S. P. Chapoval, Neuroimmune Semaphorin 4A in cancer angiogenesis and inflammation: A promoter or a suppressor? *Int. J. Mol. Sci.* **20**, 124 (2019).
27. G. M. Delgoffe, S. R. Woo, M. E. Turnis, D. M. Gravano, C. Guy, A. E. Overacre, M. L. Bettini, P. Vogel, D. Finkelstein, J. Bonnevier, C. J. Workman, D. A. Vignali, Stability and function of regulatory T cells is maintained by a neuropilin-1-semaphorin-4a axis. *Nature* **501**, 252–256 (2013).
28. J. P. Lynch, R. B. Werder, Z. Loh, M. A. A. Sikder, B. Curren, V. Zhang, M. J. Rogers, K. Lane, J. Simpson, S. B. Mazzone, K. Spann, J. Hayball, K. Diener, M. L. Everard, C. C. Blyth, C. Forstner, P. G. Dennis, N. Murtaza, M. Morrison, P. O. Cuív, P. Zhang, A. Haque, G. R. Hill, P. D. Sly, J. W. Upham, S. Phipps, Plasmacytoid dendritic cells protect from viral bronchiolitis and asthma through semaphorin 4a-mediated T reg expansion. *J. Exp. Med.* **215**, 537–557 (2018).
29. N. Riaz, J. J. Havel, V. Makarov, A. Desrichard, W. J. Urba, J. S. Sims, F. S. Hodi, S. Martin-Algarra, R. Mandal, W. H. Sharfman, S. Bhatia, W. J. Hwu, T. F. Gajewski, C. L. Slingluff Jr., D. Chowell, S. M. Kendall, H. Chang, R. Shah, F. Kuo, L. G. T. Morris, J. W. Sidhom, J. P. Schneck, C. E. Horak, N. Weinhold, T. A. Chan, Tumor and microenvironment evolution during immunotherapy with nivolumab. *Cell* **171**, 934–949.e16 (2017).
30. E. A. Akbay, S. Koyama, Y. Liu, R. Dries, L. E. Bufe, M. Silkes, M. M. Alam, D. M. Magee, R. Jones, M. Jinushi, M. Kulkarni, J. Carretero, X. Wang, T. Warner-Hatten, J. D. Cavanaugh, A. Osa, A. Kumanogoh, G. J. Freeman, M. M. Awad, D. C. Christiani, R. Bueno, P. S. Hammerman, G. Dranoff, K. K. Wong, Interleukin-17A promotes lung tumor progression through neutrophil attraction to tumor sites and mediating resistance to PD-1 blockade. *J. Thorac. Oncol.* **12**, 1268–1279 (2017).
31. K. Kersten, K. H. Hu, A. J. Combes, B. Samad, T. Harwin, A. Ray, A. A. Rao, E. Cai, K. Marchuk, J. Artichoker, T. Courau, Q. Shi, J. Belk, A. T. Satpathy, M. F. Krummel, Spatiotemporal co-dependency between macrophages and exhausted $CD8^+$ T cells in cancer. *Cancer Cell* **40**, 624–638.e9 (2022).
32. X. Gu, U. Erb, M. W. Buchler, M. Zoller, Improved vaccine efficacy of tumor exosome compared to tumor lysate loaded dendritic cells in mice. *Int. J. Cancer* **136**, E74–E84 (2015).
33. M. Ruscetti, J. Leibold, M. J. Bott, M. Fennell, A. Kulick, N. R. Salgado, C. C. Chen, Y. J. Ho, F. J. Sanchez-Rivera, J. Feucht, T. Baslan, S. Tian, H. A. Chen, P. B. Romesser, J. T. Poirier, C. M. Rudin, E. de Stanchina, E. Manchado, C. J. Sherr, S. W. Lowe, NK cell-mediated cytotoxicity contributes to tumor control by a cytostatic drug combination. *Science* **362**, 1416–1422 (2018).
34. D. Ito, S. Nojima, M. Nishide, T. Okuno, H. Takamatsu, S. Kang, T. Kimura, Y. Yoshida, K. Morimoto, Y. Maeda, T. Hosokawa, T. Toyofuku, J. Ohshima, D. Kamimura, M. Yamamoto, M. Murakami, E. Morii, H. Rakugi, Y. Isaka, A. Kumanogoh, mTOR complex signaling through the SEMA4A-Plexin B2 axis is required for optimal activation and differentiation of $CD8^+$ T cells. *J. Immunol.* **195**, 934–943 (2015).
35. H. Huang, L. Long, P. Zhou, N. M. Chapman, H. Chi, mTOR signaling at the crossroads of environmental signals and T-cell fate decisions. *Immunol. Rev.* **295**, 15–38 (2020).
36. A. Nukazuka, S. Tamaki, K. Matsumoto, Y. Oda, H. Fujisawa, S. Takagi, A shift of the TOR adaptor from Rictor towards Raptor by semaphorin in C. elegans. *Nat. Commun.* **2**, 484 (2011).
37. K. N. Pollizzi, C. H. Patel, I. H. Sun, M. H. Oh, A. T. Waickman, J. Wen, G. M. Delgoffe, J. D. Powell, mTORC1 and mTORC2 selectively regulate $CD8^+$ T cell differentiation. *J. Clin. Invest.* **125**, 2090–2108 (2015).
38. V. Bronte, P. Zanovello, Regulation of immune responses by L-arginine metabolism. *Nat. Rev. Immunol.* **5**, 641–654 (2005).
39. T. L. Bowlin, B. J. McKown, G. F. Babcock, P. S. Sunkara, Intracellular polyamine biosynthesis is required for interleukin 2 responsiveness during lymphocyte mitogenesis. *Cell. Immunol.* **106**, 420–427 (1987).
40. R. Wang, C. P. Dillon, L. Z. Shi, S. Milasta, R. Carter, D. Finkelstein, L. L. McCormick, P. Fitzgerald, H. Chi, J. Munger, D. R. Green, The transcription factor Myc controls metabolic reprogramming upon T lymphocyte activation. *Immunity* **35**, 871–882 (2011).
41. A. Zabala-Letona, A. Arruabarrena-Aristorena, N. Martín-Martín, S. Fernandez-Ruiz, J. D. Sutherland, M. Clasquin, J. Tomas-Cortazar, J. Jimenez, I. Torres, P. Quang, P. Ximenez-Embun, R. Bago, A. Ugalde-Olano, A. Loizaga-Iriarte, I. Lacasa-Viscasillas, M. Unda, V. Torrano, D. Cabrera, S. M. van Liempd, Y. Cendon, E. Castro, S. Murray, A. Revandkar, A. Alimonti, Y. Zhang, A. Barnett, G. Lein, D. Pirman, A. R. Cortazar, L. Arreal, L. Prudkin, I. Astobiza, L. Valcarcel-Jimenez, P. Zuñiga-García, I. Fernandez-Dominguez, M. Piva, A. Caro-Maldonado, P. Sánchez-Mosquera, M. Castillo-Martín, V. Serra, N. Beraza, A. Gentilella, G. Thomas, M. Azkargorta, F. Elortza, R. Farràs, D. Olmos, A. Efeyan, J. Anguita, J. Muñoz, J. M. Falcón-Pérez, R. Barrio, T. Macarulla, J. M. Mato, M. L. Martinez-Chantar, C. Cordon-Cardo, A. M. Aransay, K. Marks, J. Baselga, J. Tabernero, P. Nuciforo, B. D. Manning, K. Marjon, A. Carracedo, mTORC1-dependent AMD1 regulation sustains polyamine metabolism in prostate cancer. *Nature* **547**, 109–113 (2017).
42. R. Wu, X. Chen, S. Kang, T. Wang, J. R. Gnanaprakasam, Y. Yao, L. Liu, G. Fan, M. R. Burns, R. Wang, De novo synthesis and salvage pathway coordinately regulate polyamine homeostasis and determine T cell proliferation and function. *Sci. Adv.* **6**, eabc4275 (2020).
43. A. Haghikia, S. Jorg, A. Duscha, J. Berg, A. Manzel, A. Waschbisch, A. Hammer, D. H. Lee, C. May, N. Wilck, A. Balogh, A. I. Ostermann, N. H. Schebb, D. A. Akkad, D. A. Grohme, M. Kleinewietfeld, S. Kempa, J. Thone, S. Demir, D. N. Muller, R. Gold, R. A. Linker, Dietary fatty acids directly impact central nervous system autoimmunity via the small intestine. *Immunity* **44**, 951–953 (2016).
44. E. Kondo, H. Wakao, H. Koseki, T. Takemori, S. Kojo, M. Harada, M. Takahashi, S. Sakata, C. Shimizu, T. Ito, T. Nakayama, M. Taniguchi, Expression of recombination-activating gene in mature peripheral T cells in Peyer's patch. *Int. Immunol.* **15**, 393–402 (2003).

45. S. Kuwabara, Y. Tanimoto, M. Okutani, M. Jie, Y. Haseda, Y. Kinugasa-Katayama, T. Aoshi, Microfluidics sorting enables the isolation of an intact cellular pair complex of $CD8^+$ T cells and antigen-presenting cells in a cognate antigen recognition-dependent manner. *PLOS ONE* **16**, e0252666 (2021).
46. T. Aoshi, M. Suzuki, M. Uchijima, T. Nagata, Y. Koide, Expression mapping using a retroviral vector for $CD8^+$ T cell epitopes: Definition of a Mycobacterium tuberculosis peptide presented by H2-Dd. *J. Immunol. Methods* **298**, 21–34 (2005).
47. T. Nakatani, K. Tsujimoto, J. Park, T. Jo, T. Kimura, Y. Hayama, H. Konaka, T. Morita, Y. Kato, M. Nishide, S. Koyama, S. Nada, M. Okada, H. Takamatsu, A. Kumanogoh, The lysosomal Ragulator complex plays an essential role in leukocyte trafficking by activating myosin II. *Nat. Commun.* **12**, 3333 (2021).
48. K. Sasaki, H. Sagawa, M. Suzuki, H. Yamamoto, M. Tomita, T. Soga, Y. Ohashi, Metabolomics platform with capillary electrophoresis coupled with high-resolution mass spectrometry for plasma analysis. *Anal. Chem.* **91**, 1295–1301 (2019).
49. M. Sugimoto, D. T. Wong, A. Hirayama, T. Soga, M. Tomita, Capillary electrophoresis mass spectrometry-based saliva metabolomics identified oral, breast and pancreatic cancer-specific profiles. *Metabolomics* **6**, 78–95 (2010).
50. H. Yamamoto, T. Fujimori, H. Sato, G. Ishikawa, K. Kami, Y. Ohashi, Statistical hypothesis testing of factor loading in principal component analysis and its application to metabolite set enrichment analysis. *BMC Bioinformatics* **15**, 51 (2014).
51. B. H. Junker, C. Klukas, F. Schreiber, VANTED: A system for advanced data analysis and visualization in the context of biological networks. *BMC Bioinformatics* **7**, 109 (2006).

Acknowledgments
Funding: This study was supported by the Japan Society for the Promotion of Science (JSPS) KAKENHI JP18H05282 (A.K.), the JSPS KAKENHI JP21K07252 (S.K.), research grant from the Japan Agency for Medical Research and Development (AMED) (223fa627002h0001) (A.K.), research grant from the Japan Agency for Medical Research and Development–Frontier Outstanding Research for Clinical Empowerment (AMED-FORCE) (21gm4010007h0002) (A.K.), research grant from the Japan Agency for Medical Research and Development–Core Research for Evolutional Science and Technology (AMED-CREST) (22gm1810003h0001) (A.K.), Projects for Cancer Research by Therapeutic Evolution P-CREATE (AMED) (19cm0106335h0002) (S.K.), the Project for Promotion of Cancer Research and Therapeutic Evolution P-PROMOTE (AMED) (22ama221301h0001) (S.K.), the Practical Research for Innovative Cancer Control (AMED) (22ck0106724h0001) (S.K.), a Research Grant of the Princess Takamatsu Cancer Research Fund (S.K.), grants from The Canon Foundation (S.K.), and grants from The Mitsubishi Foundation (S.K.). This research was also supported by Otsuka Pharmaceutical Co., Ltd. **Author contributions:** Conceptualization: Y.Nai., S.K., and A.K. Methodology: Y.Nai., K.M., T.H., G.W., A.O., H.M., N.S., J.V., Y.K.-K., D.O., and K.Y. Investigation: Y.Nai., K.M., T.H., G.W., A.O., H.M., N.S., J.V., Y.K.-K., D.O., and K.Y. Visualization: Y.Nai., K.M., T.H., N.S., J.V., and K.Y. Supervision: S.K. and A.K. Writing—original draft: Y.Nai., S.K., K.Y., and A.K. Writing—review and editing: All authors. **Competing interests:** Research expenses and labor costs for Y.Nai. were contributed by Otsuka Pharmaceutical Co., Ltd. K.Y. is a board member and shareholder of KOTAI Biotechnologies Inc. N.S. and J.V. are employees of KOTAI Biotechnologies Inc. The other authors declare that they have no competing interests. **Data and materials availability:** All data needed to evaluate the conclusions in the paper are present in the paper and/or the supplementary materials.

Submitted 21 August 2022
Accepted 14 April 2023
Published 19 May 2023
10.1126/sciadv.ade0718